Title Page

Fundamental Investigations and Rational Design of Durable High-Performance SOFC Cathodes

Final Report

Reporting Period: 10/01/2012 – 03/31/2016

DOE Contract No.: FC FE0009652

DOE Project Manager: Dr. Joseph Stoffa

Prepared by

Yu Chen, Dong Ding, Tao Wei, and Meilin Liu

Center for Innovative Fuel Cell and Battery Technologies

School of Materials Science and Engineering

Georgia Institute of Technology

Atlanta, GA 30332-0245

Report Issued: June 2016

DISCLAIMER

ABSTRACT

The main objective of this project is to unravel the degradation mechanism of LSCF cathodes under realistic operating conditions with different types of contaminants, aiming towards the rational design of cathodes with high-performance and enhanced durability by combining a porous backbone (such as LSCF) with a thin catalyst coating. The mechanistic understanding will help us to optimize the composition and morphology of the catalyst layer and microstructure of the LSCF backbone for better performance and durability. More specifically, the technical objectives include: (1) to unravel the degradation mechanism of LSCF cathodes under realistic operating conditions with different types of contaminants using in situ and ex situ measurements performed on specially-designed cathodes; (2) to examine the microstructural and compositional evolution of LSCF cathodes as well as the cathode/electrolyte interfaces under realistic operating conditions; (3) to correlate the fuel cell performance instability and degradation with the microstructural and morphological evolution and surface chemistry change of the cathode under realistic operating conditions; (4) to explore new catalyst materials and electrode structures to enhance the stability of the LSCF cathode under realistic operating conditions; and (5) to validate the long term stability of the modified LSCF cathode in commercially available cells under realistic operating conditions.

We have systematically evaluated LSCF cathodes in symmetrical cells and anode supported cells under realistic conditions with different types of contaminants such as humidity, CO_2, and Cr. Electrochemical models for the design of test cells and understanding of mechanisms have been developed for the exploration of fundamental properties of electrode materials. It is demonstrated that the activity and stability of LSCF cathodes can be degraded by the introduction of contaminants. The microstructural and compositional evolution of LSCF cathodes as well as the cathode/electrolyte interfaces under realistic operating conditions has been studied. It is found that SrO readily segregated/enriched on the LSCF surface. More severe contamination conditions cause more SrO on surface. Novel catalyst coatings through

particle depositions (PrO_x) or continuous thin films (PNM) were successfully developed to improve the activity and stability of LSCF cathodes.

Finally, we have demonstrated enhanced activity and stability of LSCF cathodes over longer periods of time in homemade and commercially available cells by an optimized PNM (dense film and particles) infiltration process, under clean air and realistic operating conditions (3% H_2O, 5% CO_2 and direct Crofer contact). Both performance and durability of single cells with PNM coating has been enhanced compared with those without coating. Raman analysis of cathodes surface indicated that the intensity of $SrCrO_4$ was significantly decreased.

Table of Contents

1. INTRODUCTION

The demand for clean, secure, and sustainable energy has stimulated great interest in fuel cells for efficient energy conversion. Among all types of fuel cells, solid oxide fuel cells (SOFCs) are the cleanest, most efficient chemical-to-electrical energy conversion systems. Another remarkable advantage of SOFCs is their excellent fuel flexibility, offering potential for direct utilization of hydrocarbon fuels, coal gas, biomass, and other renewable fuels.[1-4] SOFC technologies could provide an economic bridge between the fossil fuel and hydrogen-fuel economies because they can run on fossil fuels and hydrogen.[5, 6] While small SOFC systems appear poised for commercialization in distributed generation, broad market penetration will require continuous innovation of materials and fabrication processes to prolong system lifetime and reduce cost. One technical opportunity is to enhance the durability of the cathode, which still contributes the most to performance degradation and efficiency loss in the existing SOFCs.[7]

The causes of cathode degradation include (i) coarsening of the microstructure over time; (ii) decomposition of cathode materials; (iii) chemical reaction with electrolyte during fabrication; (iv) delamination from electrolyte; and (v) contaminant poisoning.[8] To date, however, the degradation rates of real SOFC stacks are still much greater than the target set by the DOE-SECA program for commercial applications: ~ 0.2% per 1,000 hours for a lifetime longer than 40,000 hours.[9] For example, an average degradation rate as high as 1.4% per 1,000 hours has been reported for a stack using an LSCF cathode operated at 750^{o}C over 10,000 hours.[10] Poisoning effects of volatile contaminants represent a major stumbling block to the realization of a durable SOFC stack, including chromium (Cr) from typical Cr-containing interconnect materials, boron (B) from sealing glasses, and sulfur (S) from the air stream under SOFC operating conditions.[11]

In reality, it is impossible to fully prevent the exposure of cathode materials to various contaminants (e.g., Cr, H_2O, and CO_2) from cell/stack components and from the air stream. One prominent cathode degradation process is Cr-poisoning, when a typical Cr-containing material is used as the interconnect or other part in SOFC

stacks.[8] It is thus crucial to obtain a fundamental understanding of the degradation of SOFC cathodes and implement an effective approach to minimize the degradation effect. It is well accepted that, in an oxidizing atmosphere at high temperatures, volatile Cr species such as CrO_3 and $Cr(OH)_2O_2$ are generated over the Cr oxide scale intrinsic to these alloys. However, it is still unclear how these Cr-containing species interact with the cathode under realistic operating conditions, resulting in degradation in cathode performance. The deposition of Cr species is believed to be mainly due to the electrochemical reduction of gaseous Cr species to solid Cr_2O_3, which may compete with the oxygen reduction reaction. Konysheva et al[12] explained that Cr-poisoning of cathodes has a *physical* origin: the poorly conductive phases (e.g., $SrCrO_4$) with low ORR activity block the transport of oxygen species to the triple-phase-boundaries (TPBs). However, Jiang et al[13-16] proposed that Cr deposition on SOFC cathode is a non-electrochemical process, kinetically limited by nucleation reactions between the gaseous Cr species and nucleation agents (e.g., Mn and Sr). In an LSM cathode, Cr deposition is controlled by a chemical dissociation, which is initiated by the nucleation reaction between the gaseous Cr species and manganese species (i.e. Mn^{2+}). The interaction between the Mn^{2+} ions and the gaseous CrO_3 species would lead to the formation of Cr–Mn–O_x nuclei. The formation of stable Cr–Mn–O_x nuclei, in turn, accelerates the crystallization and grain growth of Cr_2O_3 oxide and $(Cr,Mn)_3O_4$ spinel phases. Similarly, in an LSCF cathode, the nucleation agent is identified to be SrO segregated to the surface of LSCF cathode, which subsequently promotes the formation of a Cr-Sr-O_x phase that accelerates the crystallization and growth of $SrCrO_4$. The formation of $(Cr,Mn)_3O_4$ on LSM and $SrCrO_4$ on LSCF resulted in performance degradation. Consequently, they proposed that cathode materials, which are free of nucleation agents (such as Mn- and Sr-containing species), would be more tolerant toward Cr deposition. A typical material, $La(Ni,Fe)O_{3-\delta}$ (LNF) was thus proposed and demonstrated to be tolerant toward Cr-poisoning in comparison to the LSM cathode in subsequent studies.[17, 18] However, Stodolny et al.[19-21] recently found that LNF was not stable when exposed to Cr-containing alloys; Ni atoms occupying the B-site can be replaced by Cr

to form a secondary phase with lower conductivity, even at a temperature as low as 600^{o}C. They attributed the inconsistency with other studies to the microstructure of the cathode, and concluded that Cr-poisoning depends strongly on cathode microstructure and operating temperatures, signifying the importance of cathode microstructures or architectures.

2. EXECUTIVE SUMMARY

Electrochemical performance of blank LSCF has been evaluated at 750 ^{o}C in the presence of different contaminants. A degradation mechanism for LSCF cathodes under realistic operating conditions with different types of contaminants has been proposed and unraveled using *in-situ* and *ex-situ* measurements. The microstructural and compositional evolution of LSCF cathodes as well as the cathode/electrolyte interfaces under realistic operating conditions have been studied. Surface segregation/enrichment of Sr is critical to LSCF degradation. We also correlated the fuel cell performance instability and degradation with the microstructural and morphological evolution and surface chemistry change of the cathode under realistic operating conditions. Enriched SrO will react with H_2O, CO_2 or Cr, to form certain insulating phases, which can block active reaction sites for ORR. Such contaminants can pull Sr out continuously from LSCF matrix. We proposed an efficient way to enhance the performance and durability of LSCF cathodes, through surface modification. A robust and conformal coating has been developed and deposited on LSCF surface. New catalyst materials and electrode structures were explored to enhance the stability of the LSCF cathode under realistic operating conditions. Capability of our best catalyst in enhancing durability of LSCF under ROC has been evaluated in both symmetrical cells, home-made single cells and commercial single cells. Our results show that, such efficient catalysts can improve performance and enhance stability of LSCF cathodes with different contaminants under operation conditions (0.7V).

The significant findings can be briefly summarized as follows:

- Established a new testing system for cells with porous electrodes, thin film electrodes, and patterned electrodes upon exposure to different contaminants, including H_2O, CO_2, and Cr;
- Characterized the electrochemical behavior of porous LSCF cathodes exposed to H_2O or CO_2, and investigated the effects of contaminant concentration and polarization condition on performance of the LSCF cathodes;
- Fabricated thin-film LSCF cells with an asymmetrical configuration, enabling

simple two-electrode testing.

- Characterized the electrochemical behavior of the thin-film LSCF cathodes exposed to H_2O or CO_2, or in direct contact with a Cr-containing interconnect, and investigated the effects of contaminant concentration and temperature on the performance of the LSCF cathodes;
- Analyzed the LSCF samples chemically exposed to H_2O, CO_2, and Cr under intermediate and aggressive conditions using surface enhanced Raman spectroscopy (SERS), and obtained important surface information. Relevant degradation mechanisms were proposed.
- Designed and implemented an *operando* SOFC testing assembly capable of characterizing the thin film LSCF cells using a synchrotron-based in situ X-ray technique.
- Identified the chemical reactions and species of the LSCF cathode resulting from high temperature exposure of CO_2, H_2O, or combination thereof using a synchrotron-based XPS technique.
- Analyzed the synchrotron-based XPS results of the LSCF thin film upon exposure to H_2O and CO_2, and obtained more comprehensive understanding about the role of specific elements in perovskite structures.
- Proposed mechanisms for how contaminants influence the LSCF performance.
- Measured the electrochemical behavior of the porous LSCF cathode exposed to H_2O and CO_2 at high levels, and established a standard procedure for new catalyst screening;
- Developed new catalyst coatings and studied their susceptibility to H_2O and CO_2, and their effect on the electrocatalytic activity of the LSCF cathode under OCV conditions.
- Examined catalyst-modified LSCF cathodes using surface enhanced Raman spectroscopy (SERS) after electrochemical testing in air contaminated with H_2O, CO_2, and Cr, and the results showed that the catalyst enhanced contaminant tolerance;

- Designed and fabricated experimental set-up for synchrotron-enabled X-ray analyses (XRD, XAS, and XPS) to study crystal structure, local atomistic structure, and electronic structure evolution of catalysts-coated LSCF cathodes in response to exposure to contaminants (Cr, H_2O, and CO_2).
- Evaluated the polarization behavior of blank and catalyst-infiltrated LSCF cathodes under accelerated conditions using electrochemical techniques and impedance spectroscopy;
- Developed an effective procedure for reliable screening of catalyst materials for mitigation of cathode degradation;
- Demonstrated some catalysts with effective tolerance to contamination poisoning of LSCF cathodes;
- Implemented DFT+U method to comparatively study the bulk and surface activity of praseodymia and ceria, validating the higher oxygen vacancy concentration and lower migration energy of praseodymia.
- Established a new testing system for single cells allowing the cathode to be exposed to different contaminants including H_2O, CO_2 and Cr;
- Applied SERS techniques to study blank and catalyst-modified LSCF cathodes after long-term performance measurements under realistic conditions.
- Systematically evaluated LSCF cathodes in *anode-supported* cells under realistic conditions with different types of contaminants such as dry/wet air with CO_2, with and without direct Crofer contact;
- Evaluated LSCF cathodes in commercial *anode-supported* cells under realistic conditions with different types of contaminants such as dry/wet air with CO_2, with direct Crofer contact

3. EXPERIMENTAL

This study includes the development of processing procedures for fabricating thin-film catalysts (e.g., PNM or other new Pr-based materials) on LSCF; characterization of the morphology, composition, and catalytic activity of these materials under realistic operating conditions; identification of the correlation between catalytic activity and morphology/composition as well as their evolution over

time; investigation into the polarization behavior and the chemical compatibility (or inter-diffusion) of the "buried" interfaces between the catalysts and the backbone under realistic operating conditions; application of our electrochemical models to the quantitative design of experiments, to the interpretation of experimental results, to the prediction of electrode performance, and to the design of new electrode structures/architecture; integration of gained knowledge into models and simulations to guide rational design of efficient cathode materials and structures of low loss and high stability; application of the knowledge to actual cells with the state-of-the-art LSCF-based cathodes, and validation of the theory and models using commercially available cells.

In order to facilitate the electrochemical evaluation of LSCF cathode with and without catalyst infiltration, we used symmetrical cells with three electrode configuration and applied a steady-state polarization to investigate the overpotential dependence of interfacial polarization resistance (*Rp*) in cathodes in contaminate containing atmospheres. We also used these cathodes in homemade full cells in order to study the long-term stability under a constant voltage (0.7 V). The cathode side was put into a closed chamber, in which different contaminants can readily be introduced. Scanning electron microscopy (SEM), transmission electron microscopy (TEM), x-ray absorption spectroscopy (XAS), and Raman spectroscopy were employed to investigate the cathode interface and the structural changes which occurred under the influence of external stimuli. The detailed structure, composition, and morphology of the LSCF surface and the catalyst/LSCF interfaces were characterized using electron microscopy (SEM and TEM) and spectroscopy. The microscopic details of the cathodes were also correlated directly with their electrochemical performance. Furthermore, a general and empirical method for designing test cells, and a semi-empirical method based on continuum modeling were developed for the interpretation of electrochemical testing results regarding the performance enhancement of the catalyst-coated LSCF cathode.

In the case of LSM, PNM, PSM and PSCM infiltration, stoichiometric amounts of high-purity praseodymium nitrate hydrate, lanthanum nitrate hexahydrate,

strontium nitrate, cobalt nitrate hexahydrate, and manganese nitrate hydrate (all from Alfa Aesar) were dissolved in a mixture of deionized water and ethanol (at a volume ratio of 1:1) to form the solutions with different concentrations. 5 wt.% polyvinyl pyrrolidone (PVP) was added to the solutions as a surfactant and stoichiometric amounts of glycine were added as a complexing agent and the fuel for subsequent self-combustion. In the case of PrOx infiltration, aqueous nitrate solutions of $Pr(NO_3)_3$ precursors with different concentrations were prepared by dissolving proper amounts of $Pr(NO_3)_3 \cdot 6H_2O$ and glycine into the distilled water. Glycine was used as a complexing agent to facilitate the phase formation. In all infiltrations, 5 μL of the stock solution was deposited on the as-prepared LSCF surface or a porous cathode (0.3 cm^{-2}) using micro-liter syringe to control the amount of loading.

The effects of catalyst infiltration on the performance of the LSCF cathodes were investigated using symmetrical and anode-supported button cells. In the configuration of a symmetrical cell, SDC pellets were prepared by uniaxially pressing a commercially available SDC powder (Fuel Cell Materials, US) followed by sintering at 1450 ^oC for 5 h to achieve relative density of ~98%. LSCF (Fuel Cell Materials, US) green tapes were prepared by tape-casting, which were then bound onto both sides of a SDC electrolyte pellet using a slurry of $Sm_{0.2}Ce_{0.8}O_{2-\delta}$ (the buffer layer). The SDC powder was synthesized using a chemical co-precipitation process [22, 23]. The SDC powder was then dispersed in acetone with V-006 (Heraeus, US) as binder and ball-milled for 24 h to form a stable SDC slurry. The cells were then co-fired at 1080^oC for 2 h to form porous LSCF electrodes (with an area of 0.3 cm^2) on SDC. The symmetrical cells were also tested in a three-electrode configuration. The LSCF cathode with/without catalyst coating were used as working electrode (WE) and counter electrode (CE), respectively. Pt paste was fired at 900^oC for 1 h as reference electrode (RE) by positioning it as close to working electrode as possible. In the configuration of an anode-supported cell, tape-cast NiO/YSZ anode-support was first fabricated and pre-fired at 850^oC for 2 h. Then, an active NiO/YSZ layer (~15 μm) and a YSZ electrolyte (~15 μm) were sequentially deposited on the anode support by a particle suspension coating process followed by co-firing at 1400^oC for 5 h [38].

The cell size is about 10 mm in diameter. The LSCF cathode was then applied to the YSZ electrolyte using the same procedures as described in the fabrication of symmetric cells. The commercial button cells provided by MSRI are 10 mm in diameter with an active cathode area of 0.3 cm^2. The cell configuration is a conventional anode (NiO/YSZ)-supported electrolyte (YSZ) film. LSCF is used as the cathode material while SDC is employed as a barrier layer between electrolyte and cathode. LSCF/SDC is the cathode interlayer between LSCF and barrier layer. The infiltration processes were optimized by adjusting the composition of the solvent, pH value of the solution, and modifying the surface properties of the cathode. To accurately control the PNM loading, we applied poly-(alkylene) carbonates (QPAC) to prevent the solution from spreading outside the LSCF cathode. To maximize the performance improvement, we used PNM solution with different concentrations at a fixed volume to infiltrate the commercial cells. A long-term electrochemical test was performed on the infiltrated cells for ~550 hours, to comparatively study the extent of performance enhancement. When a series of optimal infiltration parameters were determined, a long-term electrochemical characterization at a constant voltage of 0.7 V at 750^oC was performed to observe the durability of the commercial cells with and without catalyst infiltration. After testing, SEM was employed to investigate the surface, bulk, and interface of the cathode. The detailed structure and morphology of the LSCF cathode were characterized. Also, the phase and structure of the cathode were analyzed by Raman spectroscopy [24].

4. RESULTS AND DISCUSSIONS

4.1 Polarization resistance (R_p) or stability change of LSCF cathode upon exposure to H_2O, CO_2 and Cr-containing materials.

Effect of water vapor concentration on Rp under OCV

The impedance spectra of LSCF in humidified air with different concentrations of water vapor (0, 3, 5, and 10%) under OCV are shown in **Figure 1**. It appears that all of the spectra display three depressed arcs, implying that at least three different electrode processes make significant contributions to the resistance associated with the oxygen reduction reaction. Note that the high and medium frequency arcs are

partially overlapped. Compared with those of the LSCF cathode fed with dry air, the medium and low frequency impedance arcs of the LSCF cathode exposed to wet air both increased with the addition of H_2O, resulting in an increase in R_p. The variation in R_p is visible even at a low H_2O level of 3% and increases with water vapor concentrations. The polarization resistance variation percentage (ΔR_p) values are shown in **Table 1**. As the water vapor concentration increases to 10%, a relatively high ΔR_p of 7.84% was observed.

The effects of different H_2O concentrations on the EIS of the LSCF cathode while under cathodic polarization were investigated. We applied a constant current density of -500 $mAcm^{-2}$ to the cell and recorded the impedance spectrum when the polarization response achieved steady state. Compared with the impedance spectra shown in **Fig. 1**, there are only two depressed arcs in the impedance spectra shown in **Fig. 2**. Moreover, the impedance loops related to low frequency increase in size with increasing water vapor concentration, while those associated with high frequency kept constant. In the literature, there is an agreement to attribute the arc associated with high frequency to the process of oxygen ion incorporation into the electrolyte while those related to medium/low frequency are usually proposed to be associated with surface reaction processes such as surface diffusion or surface adsorption and dissociation [25-27]. In our present study, the effects of water vapor on the EIS of the LSCF cathode, either under OCV or under polarization, are evidenced to be possibly related to the surface processes. This finding through electrochemical characterization is in good agreement with the observation that the increase of the surface exchange rate is more pronounced at higher water partial pressure, so surface and hydroxide species may play an important role in the oxygen surface exchange process. This also suggests the importance of surface modifications or decorations to suppress or eliminate the negative effects of water vapor on the performance of the LSCF cathode.

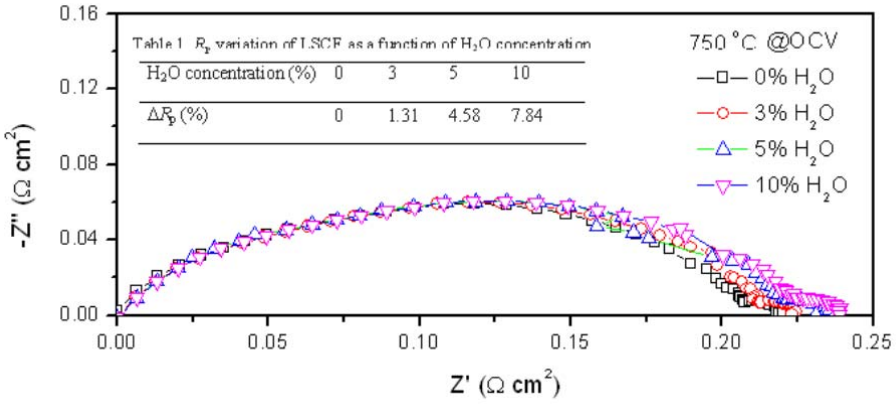

Figure 1 The impedance spectra of the LSCF cathode in humidified air with different concentrations of water vapor (0, 3, 5, and 10%) under OCV at 750℃.

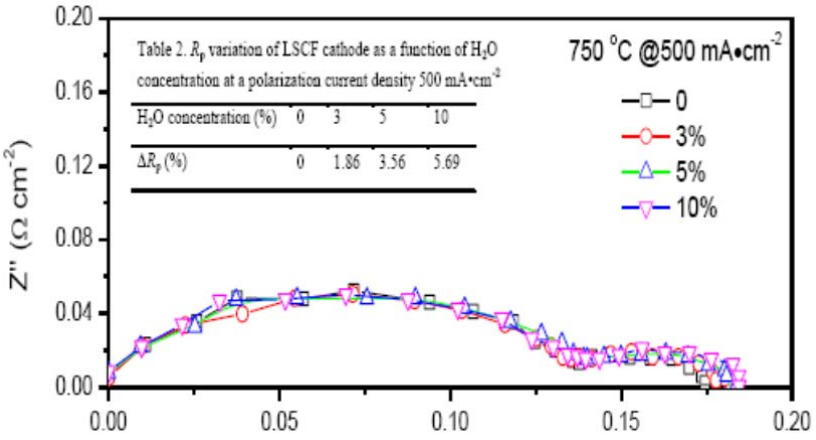

Figure 2 Impedance spectra of LSCF in air with various water vapor concentrations (0, 3%, 5% and 10%) at a cathodic current density of 500 mAcm^{-2} at 750 °C.

We also performed a polarization test with a constant cathodic current density of 500 mAcm^{-2}, during which the concentration of water vapor was varied. The overpotential of the LSCF in air with different concentrations of water vapor is shown in Figure 3. The change in the overpotential is not significant for LSCF cathode when the concentration of water vapor is low (3% and 5%), as shown in Figure 3a. However, a noticeable performance change was observed when 10% water vapor was fed in. More interestingly, switching back from wet to dry air resulted in a reversible decrease in the magnitude of the overpotential, indicating that the performance loss of the LSCF cathode was recoverable after the water vapor was removed from air in the

short term. This implied that H_2O may be physically adsorbed onto the surface of the cathode, and it could be easily removed during a short period.

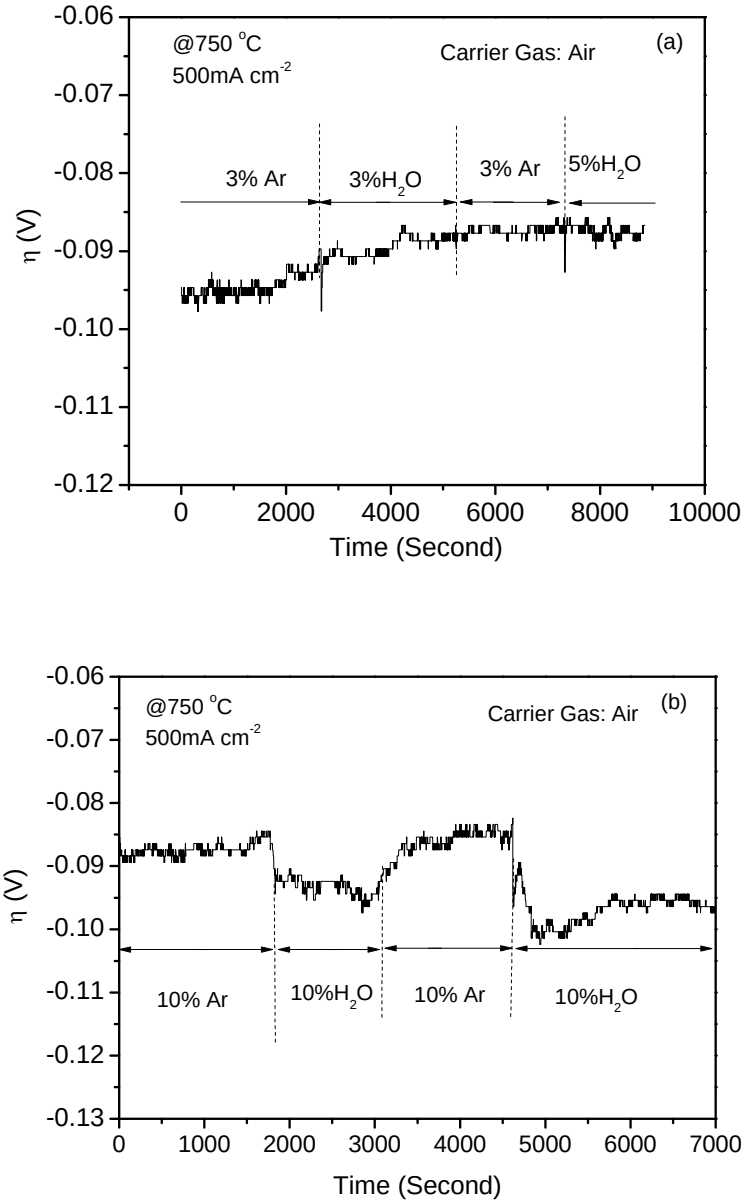

Figure 3 Overpotential of LSCF in air with different amounts of 3% (a) and 10 % H_2O (b).

At 750°C, the Rp gradually increased with H_2O content in air and degree of increase was still relatively small even when the concentration of H_2O is increased up to 10%.

This trend is the same trend observed in our previous report (**Figure 4a**). However, the Rp change exhibited a noticeable difference when the temperature was reduced to 600°C. As shown in **Figure 4b**, the R_p increased rapidly with the addition of 3% H_2O while further increase of H_2O content showed little effect on further increase of R_p. The *Rp* rapidly increases when 3 % water vapor was added. Further increase in water content has little effect on *Rp* increase, suggesting that the adsorption of water vapor preferentially occupied the active site of the LSCF surface and that it is more likely to reach full coverage at lower temperature with low concentration of water vapor (**Figure 5**).

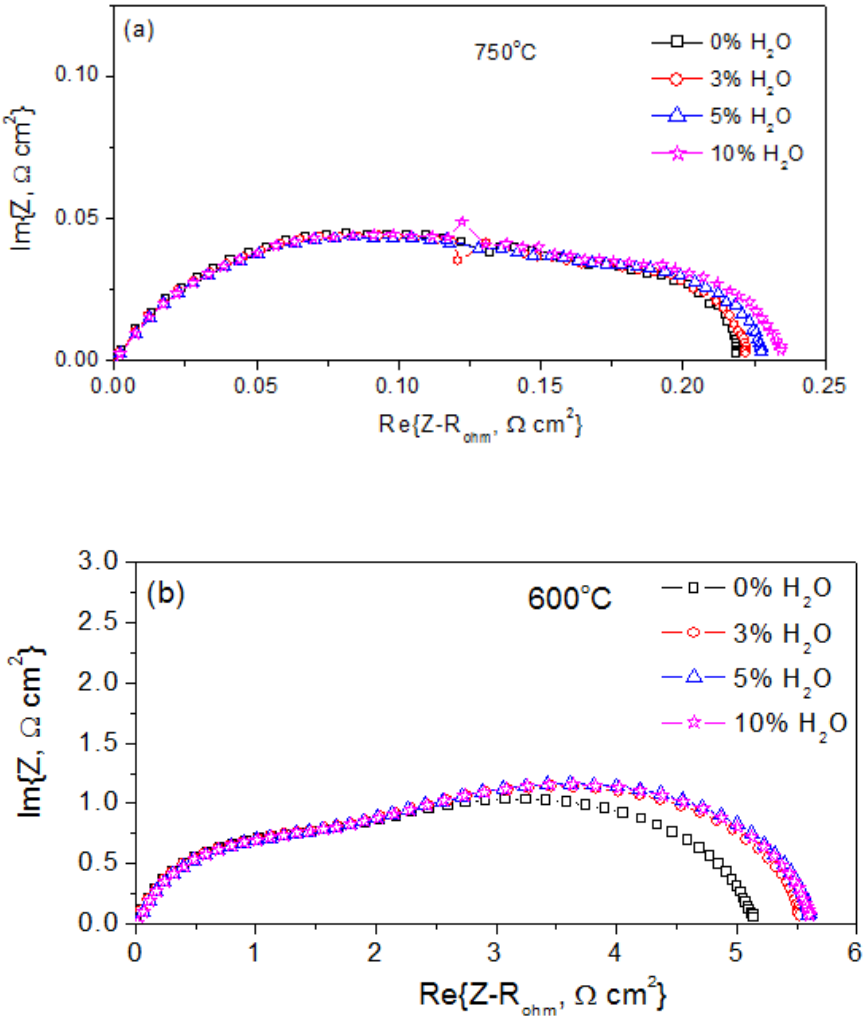

Figure 4 The impedance spectra of the porous LSCF cathode in humidified air with different concentrations of water vapor (0, 3, 5, and 10%) under OCV at 750 °C (a)

and 600 °C (b).

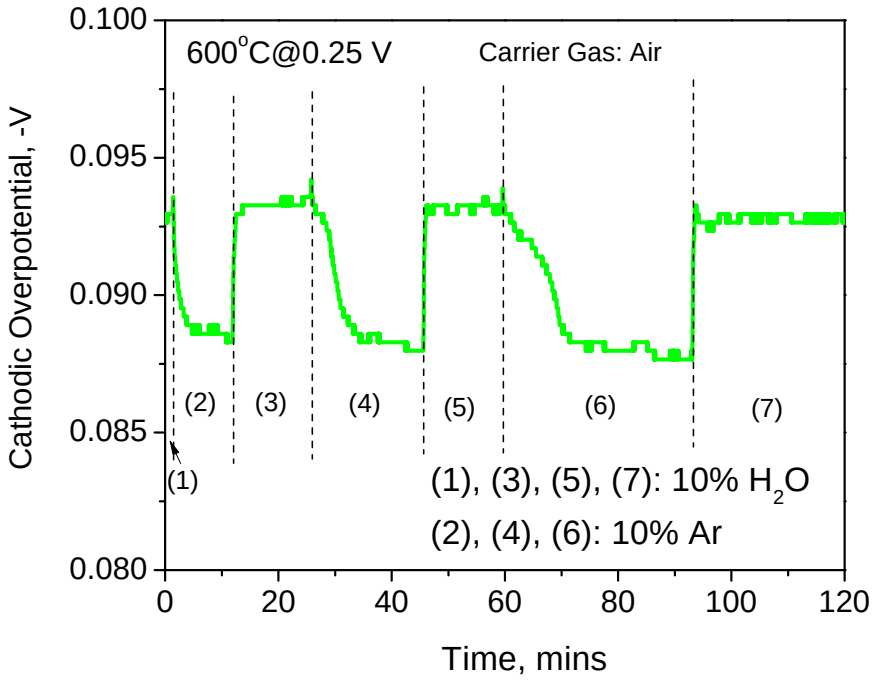

Figure 5 Overpotential of an LSCF cathode in air with switching between 10% argon and water vapor under a constant voltage of 0.25 V at 600 °C.

The degree of *Rp* increase did not show significant temperature dependence. When the temperature is as low as 600 °C, the percentage of *Rp* increase is comparable to that at 750 °C when exposed to 10 % water vapor. Under OCV condition, the cathodic polarization resistance (Rp) of the LSCF cathode increases with the concentrations of H_2O and CO_2. The degree of Rp increase is larger at lower temperatures but tends to be similar at high concentrations of H_2O and CO_2.

Table 1 The increased percentage in R_p of the LSCF cathode when exposed to different concentrations of water vapor at 600 and 750 °C.

Temperature	**Water vapor concentration (%)**		
	3% H_2O	**5% H_2O**	**10% H_2O**
600°C	7.1 %	8.4 %	8.7 %
750°C	1.9 %	5.4 %	8.5 %

The polarization behavior of the LSCF cathode was reversible when the gas was switched from dry air (with 10% argon) to wet air (with 10% water vapor) during a short period of time. However, it needed a progressively longer time to recover, implying possible reconstruction on the surface of the LSCF cathode when exposed to H_2O at low temperatures (**Figure 5**).

Under a cathodic polarization, the overpotential increase of the LSCF cathode is more sensitive to CO_2 than to H_2O at 600 ^oC while H_2O may play a more prominent role than CO_2 at 750 ^oC. The combined effect of H_2O and CO_2 on the overpotential increase is similar to the sum of the individual ones, suggesting that the instant effect of H_2O and CO_2 on performance change may be independent.

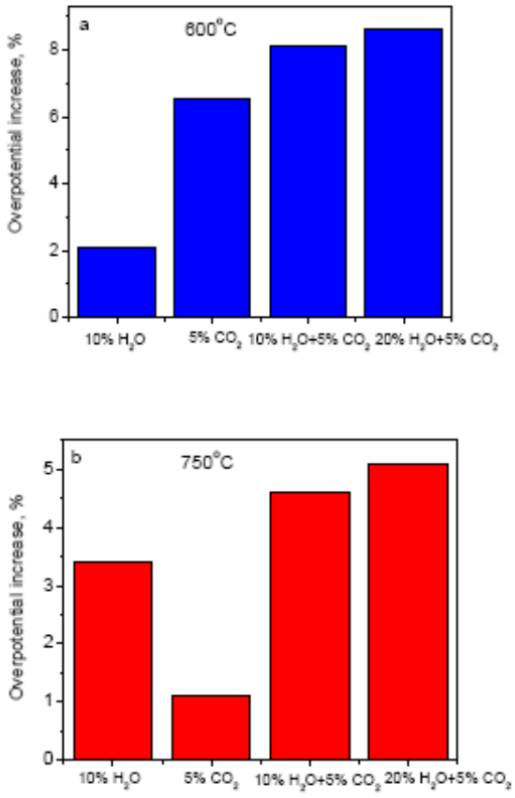

Figure 6 Overpotential change of LSCF cathodes exposed H_2O and CO_2 at different temperature: (a) 600 ^oC; (b) 750 ^oC.

Effect of CO_2 on R_p

The change in the polarization resistance (*Rp*) is not distinguishable at concentrations of CO_2 lower than 3 % under OCV. Similar to the electrochemical tests involving air containing H_2O, we performed identical electrochemical characterization on the LSCF cathode exposure to air containing CO_2. Under OCV condition, the change in R_p became visible when the concentration of CO_2 was increased to 5%, and the percentage change in R_p is approximately 9.0%. However, when we applied a constant cathodic current density of 500 mA cm^{-2} to the cells, it is clear that the impedance spectrum arc appeared to change, even when the concentration of CO_2 is as low as 3 vol%, as shown in **Figure 7**. It seems that the polarization can exacerbate the effect of CO_2, which is similar to the case of the LSCF cathode with humidified air.

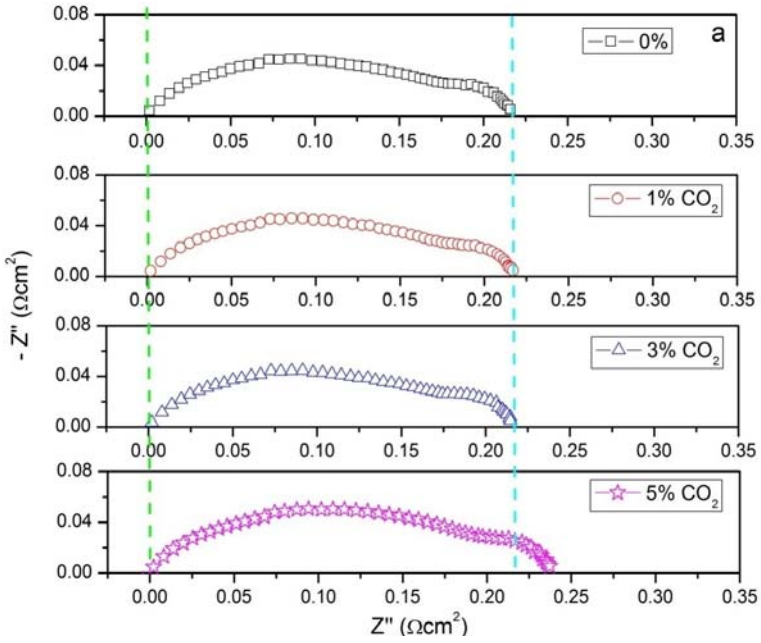

Figure 7 Impedance spectra of the LSCF cathode in air with various CO_2 concentrations (0, 1%, 3%, and 5%) under OCV at 750 ^oC.

Under a polarization current density of 500 $mAcm^{-2}$, the *Rp* showed a small increase when 3% of CO_2 was added (**Figure 8**). We also monitored the polarization behavior when the air with 3% argon was switched to the air with 3% CO_2. The overpotential of LSCF at 750^oC in air with 3% argon or CO_2 was recorded over time, as shown in **Figure 9**. The change in the overpotential is obvious for the LSCF cathode when the

atmosphere is changed from air with 3% argon to the air with 3% CO_2. Switching back to air with 3% argon resulted in a reversible decrease in the magnitude of the overpotential, indicating that the performance loss of LSCF can be recovered with the removal of CO_2 in the short term. This behavior is similar to what we observed in the case of H_2O in air.

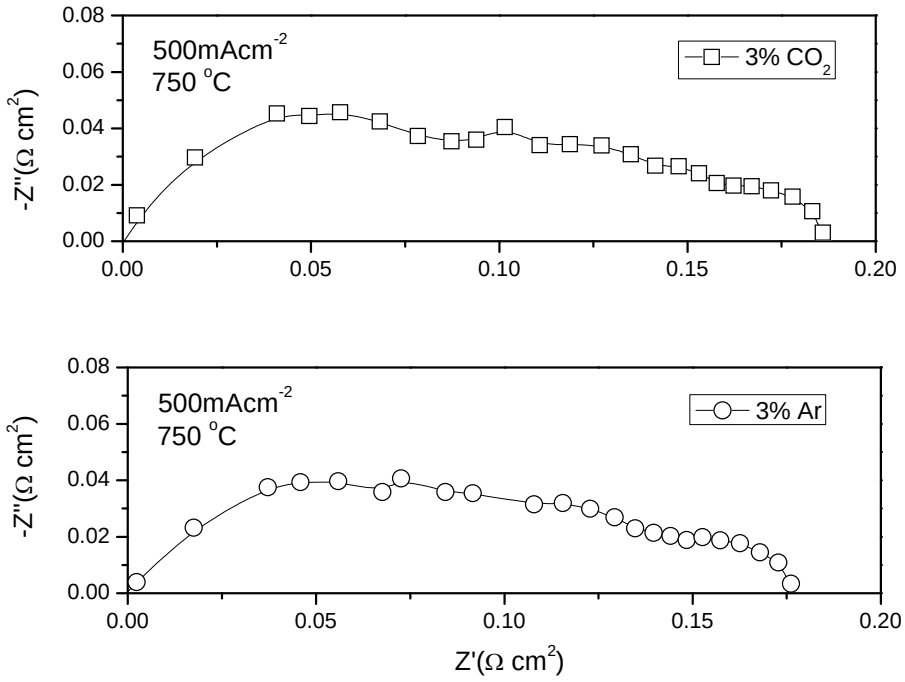

Figure 8 Impedance spectra of the LSCF cathode in air with 3 % CO2 or argon with a constant cathodic current density of 500 $mAcm^{-2}$ at 750 ^oC.

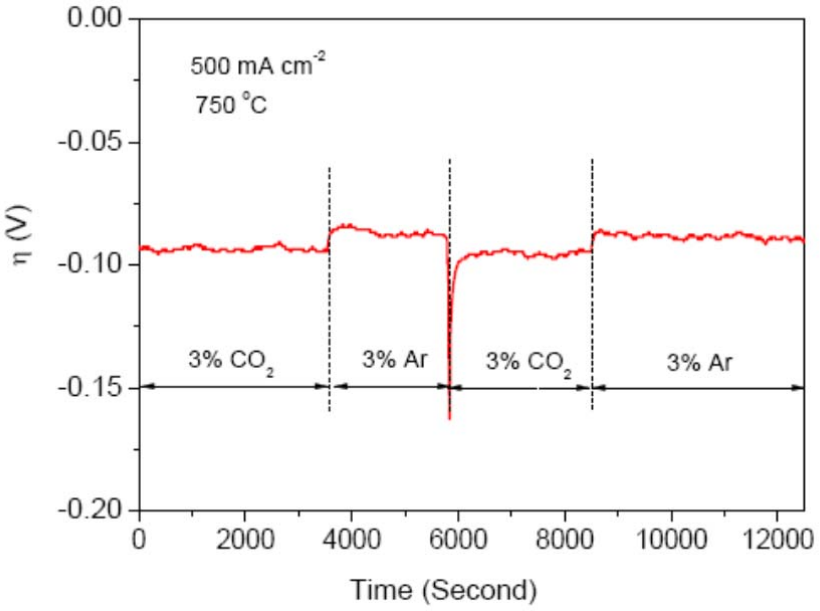

Figure 9 Overpotential of LSCF cathode in air with and without 3% CO_2 at a constant cathodic current density of 500 $mAcm^{-2}$ at 750 ^oC

In order to further investigate the poisoning effect of CO_2 on the LSCF cathode over time, the overpotential at a current density of 500 $mAcm^{-2}$ was recorded, as shown in **Figure 10**. It appears that the LSCF did not exhibit a gradual degradation at a short term. This suggests that the addition of CO_2 would not cause a time-dependent degradation in the short term.

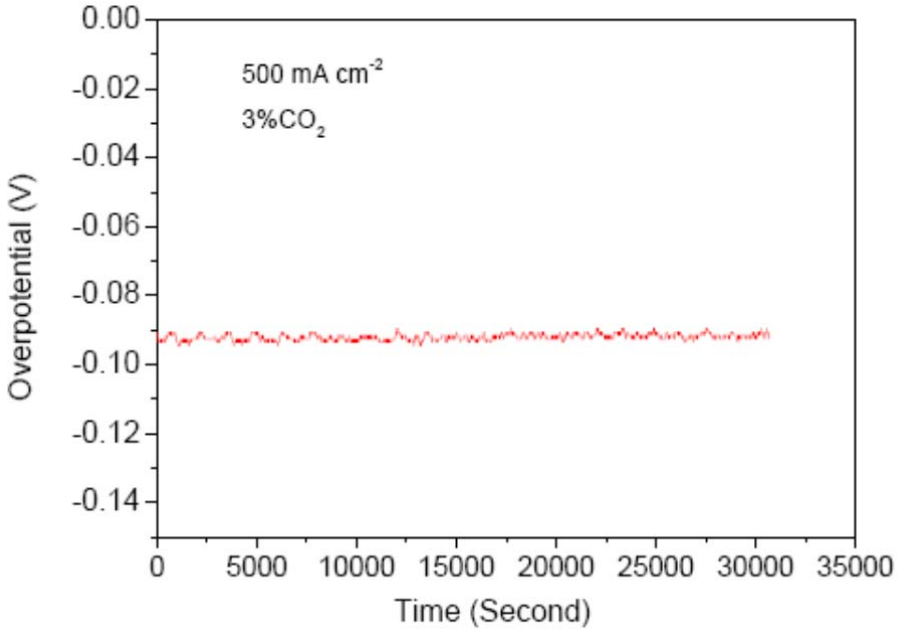

Figure 10 Overpotential of the LSCF cathode as a function of time in air with 3% CO_2 tested at 750 ^{o}C.

Effect of Cr poisoning

Investigation of Cr poisoning and the development of Cr-tolerant materials is another objective of this project (in addition to studying the effects of H_2O and CO_2). This is because metallic materials are the preferred choice for interconnects over a ceramic counterpart because of their higher electronic conductivity, better mechanical properties, higher thermal conductivity, and lower cost [28-30]. However, these interconnect materials could be the main sources of Cr poisoning in SOFC cathodes, resulting in severe degradation in performance. Thus far, Cr poisoning of $La_{1-x}Sr_xMnO_{3-\delta}$ (LSM) cathodes has been widely studied above 750^{o}C [13, 31, 32], and there are a few reports of Cr poisoning on LSCF cathodes at lower temperatures [33]. Researchers are putting more efforts into understanding the effect of Cr poisoning on long term stability of SOFC cathodes. In the present study, our objectives are to investigate the effect of Cr on the performance of the LSCF cathode with different water vapor concentrations and with the different exposure approaches, such as by introducing Cr vapor or by making direct contact with Cr-containing materials. We will use a similar method, as described in the last report, to monitor the

performance change due to contamination, which is based on the same cell tested under the same conditions. The data are thus still free from variations in the performance from cell to cell.

We used a three-electrode configuration to evaluate the symmetrical cells exposed to gases containing different concentrations of contaminants. All cell components and the fabrication processes are the same as those described in the experimental section. A commercially available alloy was used as the interconnect material: Crofer 22 APU (20-24% Cr, 0.3-0.8% Mn, 0.5% Si, 0.03% C, 0.5% Al, 0.02% S, 0.05% P, 0.03-0.20% Ti, 0.04-0.20% La and the remaining Fe, Fuelcell Materials, USA). The alloy was cut into coupons (7 mm × 7 mm× 0.1 mm) and then placed on the side of one electrode. As shown in Error! Reference source not found.a, the LSCF electrode in direct contact with the interconnect material is used as the working electrode (WE) to monitor the change in performance of this electrode due to direct contact with the interconnect materials (Cr-poisoning due to surface or solid-state diffusion). Subsequently, we used the other LSCF electrode, which was not in direct contact with the interconnect material, as the WE (as schematically shown in **Figure 11b**) to monitor the change in performance of the electrode due to exposure to Cr-containing gas (Cr-poisoning due to Cr transport through the gas phase). Our objective is to study the effect of Cr-poisoning due to different transport mechanism using a single cell.

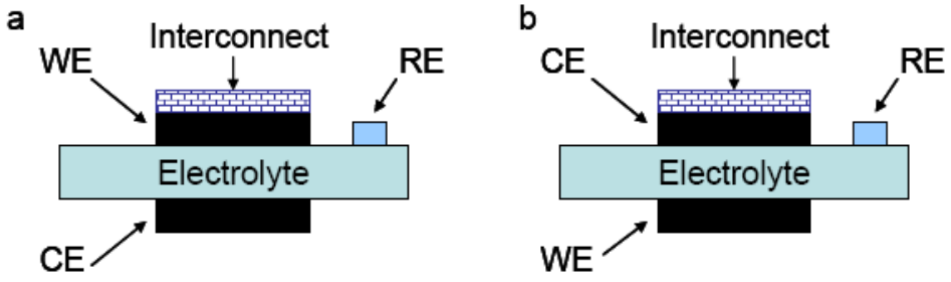

Figure 11 A schematic of the symmetrical cells with a three-electrode configuration used in this study: (a) the working electrode in direct contact with the Cr-containing interconnect material and (b) the working electrode is not in direct contact with the interconnect material.

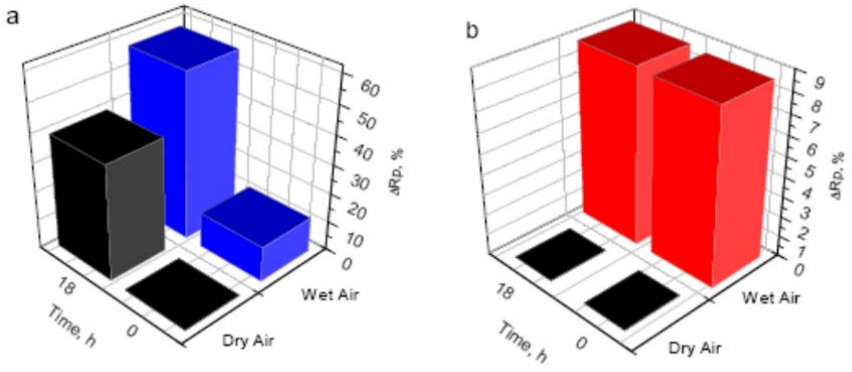

Figure 12 Variation in Rp of an LSCF cathode in dry air and wet air (20% H_2O) with time under OCV condition for a) the electrode in direct contact with the interconnect shown in Figure 11a; b) the electrode away from the interconnect shown in Figure 11b.

Shown in Error! Reference source not found.**a** are variations in R_p with addition of water vapor for the LSCF electrode in direct contact with the interconnect at different time under OCV conditions (see the electrode configuration shown in Error! Reference source not found.a). We first measured the impedance spectra in dry and wet (20% H_2O) air, and then the system was switched back to dry air and held there for 18 hours. We then performed similar measurements to determine the time dependence of R_p under the same conditions. It is clear that R_p initially increased by 12.1% with the addition of water vapor. A subsequent increase of 39.6% in R_p occurred during the subsequent18-hour of holding in dry air. With the re-introduction of water vapor, R_p increased further by 57.7%. In sharp contrast, when the LSCF cathode (the WE) was not in direct contact with the interconnect material, the increase in R_p was only 8.6% with the addition of water vapor at the beginning, and this value remained the same during the 18-hour holding in dry air. The R_p value changed slightly (8.7%) when water vapor was added a second time. These results indicate that the degradation of the LSCF cathode is very sensitive to the way in which the Cr species transported to the LSCF cathode. When the LSCF electrode was not in direct contact with the interconnect, the degradation mechanism is dominated by a gas-phase

transport of Cr , for the following reasons: 1) the extent in R_p increase is comparable to our previous results, the only effect of water vapor on R_p; and 2) no visible additional degradation during the time-dependent experiment. When the electrode was in direct contact with the interconnect, the addition of water vapor may exacerbate the Cr poisoning by enhancing surface or solid-sate diffusion of Cr to the LSCF electrode. The details of the poisoning mechanism are yet to be determined.

Like our previous study of H_2O and CO_2, we also monitored the polarization behavior when the air with 20% argon was switched to air with 20% H_2O, as shown in Error! Reference source not found.. A more significant change in the overpotential is observed with switching in comparison with the case of H_2O and CO_2, which could be associated with a complex effect from both increased H_2O concentration and Cr poisoning. In contrast to the results in the case of H_2O and CO_2, a gradual decrease in overpotential is visible when H_2O is added in the presence of the interconnect. This suggests that Cr poisoning has a continuous effect on the LSCF performance, resulting in a pronounced degradation. Moreover, this effect seems to still play a role when wet air was switched back to dry air, which leads to an irreversible electrochemical process. This is characterized by a gradual increase in initial overpotential when wet air is switched back to air containing 20% Ar.

In order to further investigate the poisoning effect of the interconnect in wet air on the LSCF cathode over time, the overpotential at a current density of 500 $mAcm^{-2}$ was recorded for 18 hours, as shown in Error! Reference source not found.. Compared with a relatively constant overpotential in the case of CO_2, the LSCF cathode exhibits a significant degradation in the short term.

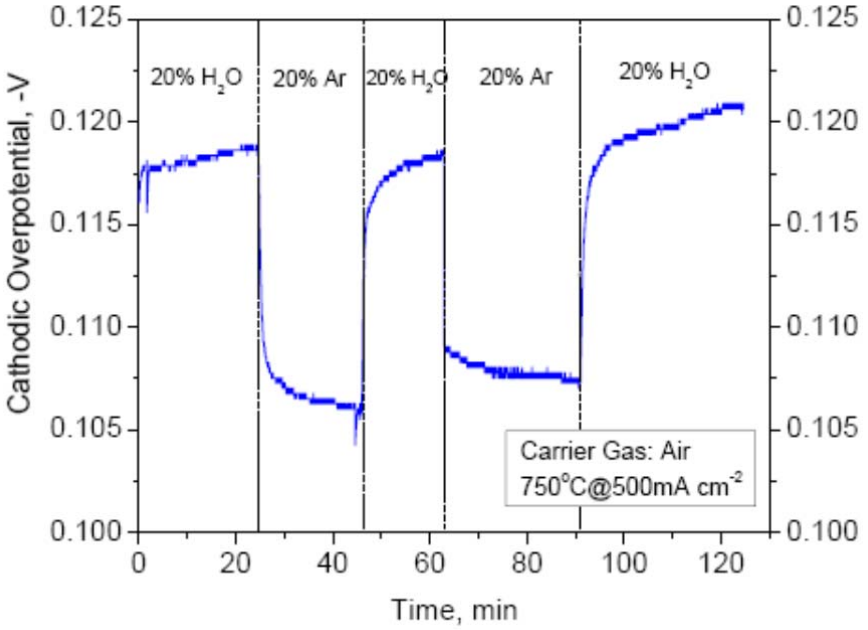

Figure 13 Overpotential of the LSCF cathode in direct contact with the interconnect in air with 20% of argon and H_2O at 750 ^oC with a constant current density of 500 mA cm^{-2}.

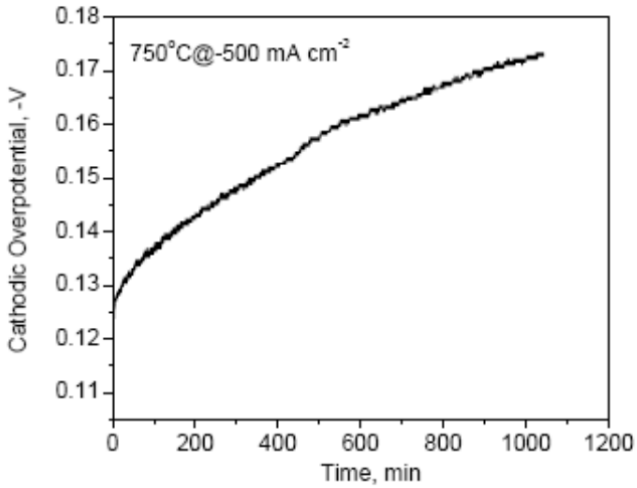

Figure 14 Overpotential of the LSCF cathode in direct contact with the interconnect in air with 20% H_2O at 750 ^oC with a constant current density of 500 mA cm^{-2}.

2.2 Characterization of the electrochemical behavior of thin film LSCF electrodes upon exposure to air containing water vapor (H_2O), to carbon dioxide (CO_2), or in direct contact with Cr-containing materials

In the previous report, we presented our results on the fabrication of the LSCF thin film through a RF sputtering technique. With partial optimization of technique parameters, we were able to obtain an LSCF thin film with the desired composition and thickness. In the present work, we used this technique to fabricate asymmetrical cells which are composed of a porous LSCF electrode that serves as the counter electrode, a dense thin film LSCF electrode that serves as the working electrode, and a thick electrolyte (GDC), as shown in **Figure 15**. Dense GDC pellets were fabricated by dry-pressing GDC powders (Daiichi, Japan) at 300 MPa and sintering at 1450^{o}C for 5 hours. A polishing process was applied to one side of the GDC pellet and LSCF ink was screen-printed on the other side and followed by firing at 1080^{o}C for 2 hours to form a porous LSCF electrode as the counter electrode. A dense LSCF thin film was sputtered on the polished side and annealed at 800^{o}C for 1 hour. Since the counter electrodes are highly porous, the polarization resistance is much smaller than that of the thin film LSCF electrodes. Thus, the electrochemical response of the asymmetrical cell is dominated by the thin film LSCF electrode. This enables us to use a simple two-electrode configuration to characterize the electrochemical behavior of the thin film electrode.

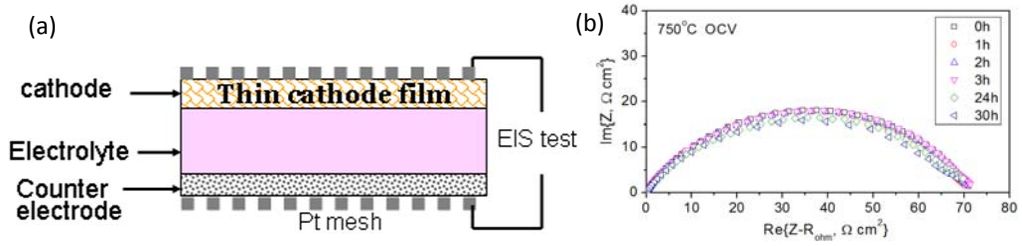

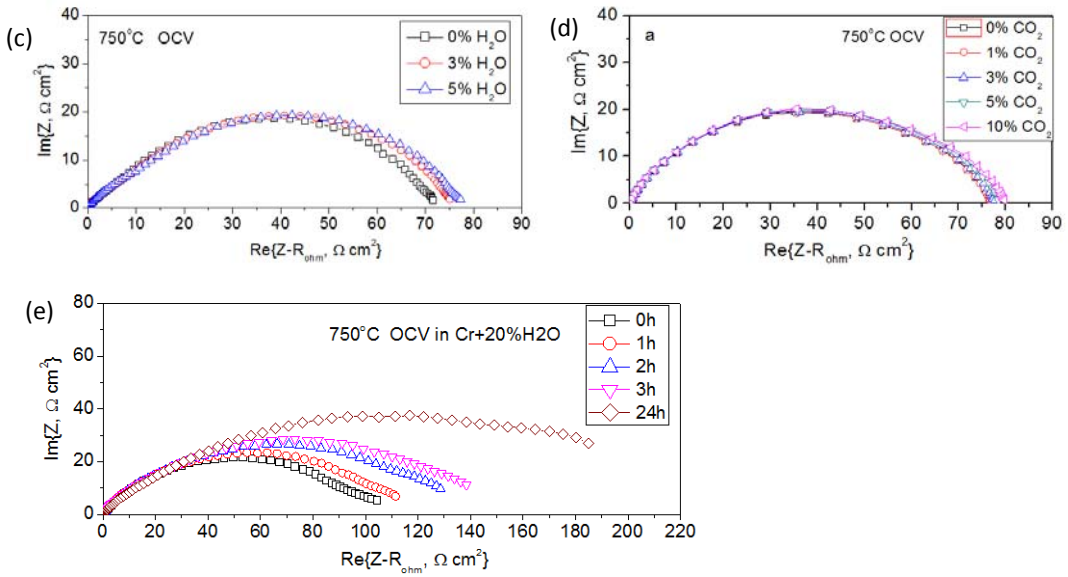

Figure 15 A schematic of the thin film cell with an asymmetrical configuration (a). Impedance spectra of thin film LSCF electrode in air at 750°C under OCV condition (b), varied vapor content (c), CO2 content and Cr (d), and time dependence of impedance spectra of the LSCF cathode in direct contact with the interconnect in wet air (20% H_2O) under OCV at 750°C

We first monitored the stability of the thin film electrode with air. As shown in **Figure 15b**, Rp, which comes from the intercepts at the high and the low frequencies in the spectrum, are approximately the identical after 30 hours, although the shapes of the arc present a slight change.

The impedance spectra of thin film LSCF in humidified air with different concentrations of water vapor (0, 3, and 5%) under OCV are shown in **Figure 15c**. It is clear that all of the spectra display two depressed arcs, implying that at least two different electrode processes make significant contributions to the resistance associated with the oxygen reduction reaction. Similar to those of the porous LSCF cathode under the same conditions, the high frequency impedance arcs have the same shape and size while the low frequency impedance arcs of the LSCF cathode exposed to wet air increased with the concentration of H_2O, resulting in an increase in R_p. Also, the increase in R_p (ΔR_p) is still relatively small (4-7%), implying that the effect of H_2O on performance is not significant in the short term.

As with the electrochemical tests involving air containing H_2O, we performed identical electrochemical characterizations on the thin film LSCF cathode exposed to

air containing CO_2. As shown in **Figure 15d**, R_p has a slight change at 750°C even if the concentration of CO_2 was increased to 20%, and the change in R_p is still lower than 6.0% under OCV condition. These results are very similar to Zhao's finding in $La_{0.6}Sr_{0.4}CoO_{3-\delta}$ [34], which might be associated with the competitive adsorption between CO_2 and O_2 on the surface of the electrode. With reduced temperatures, the former appears more dominant. More significant response in performance with reduced temperature will thus provide us a new direction in designing the new material screening procedure to mitigate the effect of CO_2 and H_2O, given the fact that the performance response is not significant at high temperatures.

We also monitored the time dependence of impedance spectra of the thin film electrode in direct contact with the interconnect and also exposed to 20% H_2O. A visible increase in R_p occurred with time, suggesting a severe degradation. The degradation level is over 100% in 24 hours. This also indicates that the mechanism of Cr poisoning is much different with that of H_2O and CO_2, especially in the presence of high content of H_2O.

2.3 Microstructural and compositional evolution of LSCF cathodes

Raman analysis of LSCF materials chemically exposed to air containing water vapor (H2O), to air containing carbon dioxide (CO_2), or in contact with chrome (Cr)-containing materials

The low signal intensity of Raman spectroscopy makes it difficult to detect the surface species present in trace amounts or to track the formation of surface species with short lifetimes. This problem becomes more severe when studying SOFC materials under realistic operating conditions because many ceramic phases possess weak Raman modes and all Raman peaks broaden at high temperatures. Surface enhanced Raman scattering (SERS) is a promising solution to this problem. Our previous study demonstrated the utility of SERS for SOFC-related materials such as deposited carbon, CeO_2, $La_{1-x}Sr_xMnO_{3-\delta}$ (LSM), and LSCF following the deposition of Ag nanoparticles on the electrode [35]. The sensitivity towards surface species is greatly enhanced upon the application of Ag nanoparticles, which provide a clean and background-free SERS effect. Due to the near field nature of SERS, the enhanced

signal mainly comes from the surface of the inspected materials, which is a unique advantage for identifying the species only present on the electrode surface.

The LSCF powders were pressed into pellets and fired at 1080°C for 10 hours. The pellets were then annealed in a variety of atmospheres to form surface contaminations. The first batch of samples were annealed in relatively moderate conditions (pure Ar, 1% O_2, pure O_2, 1% CO_2, and 3% H_2O). To make the contamination signals more notable, aggressive contamination exposures were subsequently implemented, using ambient air, 10% H_2O, 5% CO_2, and 3% H_2O with Cr. The Cr contamination was introduced by placing a Cr alloy bar and LSCF pellet in the same furnace chamber. To activate the LSCF pellets for SERS, a thin layer of silver nanoparticles was sputter-deposited (180 seconds at 8 W) on the samples. The sample preparation steps are illustrated in **Figure 16.** Finally, Raman spectra were obtained using a Renishaw RM 1000 spectromicroscopy system with an approximately 2 µm spot size. Argon laser emission lines at 514 nm were used for the excitation of Raman signal in this study, and all spectra were collected using a laser power of 15 mW.

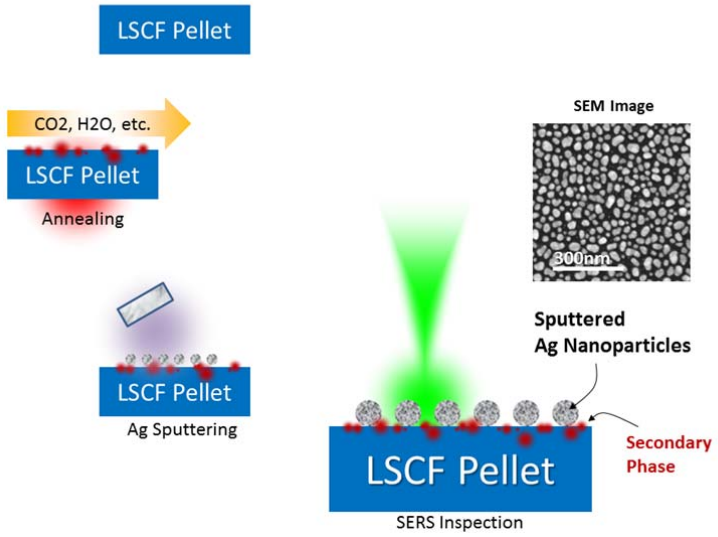

Figure 16 The schematic of surface enhanced Raman spectroscopy analysis of the degradation of LSCF surface.

The sputtered Ag enhanced the LSCF peaks significantly. As shown in **Figure 17**, the normal Raman of pristine LSCF pellets showed three strong modes (180, 320, and 720 cm^{-1}) and three weak modes (540, 950, and 1130 cm^{-1}) within the inspection range. After applying Ag nanoparticles, all Raman modes were enhanced by about 100 times. The relative peak intensity changed, but no new peaks were observed. This suggests that the Ag nanoparticles effectively enhanced the Raman signal. Since Ag particles have no active Raman modes per se, they do not introduce any extra peaks to the Raman spectrum.

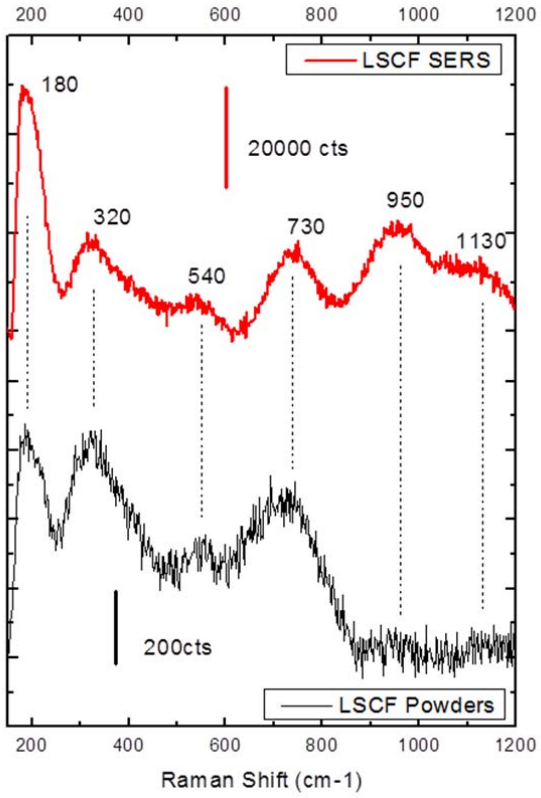

Figure 17 The Raman and SERS spectra of the pristine LSCF powders.

The LSCF pellets annealed under moderate atmospheres were inspected by both Raman and SERS technique. The normal spectra (not presented) of the LSCF pellets showed no notable difference. Presented in **Figure 18a** are the SERS enhanced spectra of the LSCF pellets. Even with the enhancement given by Ag nanoparticles, the difference in the Raman signals of the LSCF samples annealed under various

atmospheres was not easily identifiable. To magnify the difference, the SERS spectrum of pristine LSCF sample was subtracted from all sample spectra. As displayed in **Figure 18b**, the annealing in Ar, in 1% O_2, and in O_2 did not incur any identifiable change on the LSCF surface. However, the LSCF samples annealed in 1% CO_2 and in 3% H_2O showed slight increases in the 500-600 cm^{-1} range. According to the previous studies, the emerging of Raman modes in this range indicates the formation of phase with space group Pbmn [36]. However, the differences in this dataset are too weak to draw any firm conclusions.

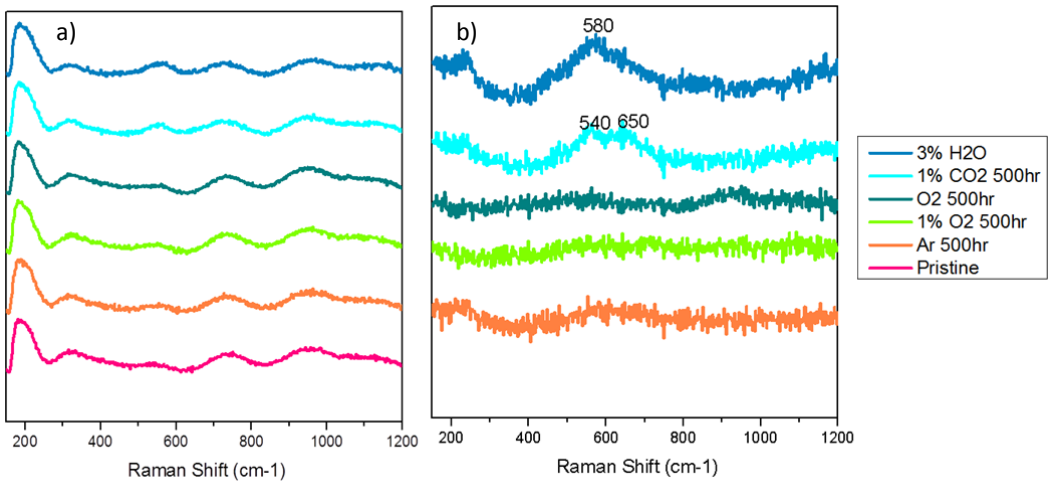

Figure 18 SERS analysis of the LSCF pellets annealed under moderate conditions: a) SERS spectra and b) SERS difference spectra with respect to the pristine condition (see context).

In order to distinguish features of the surface contaminations on the LSCF surface, the pellets were heated in more aggressive gas atmospheres. Shown in **Figure 19** are the normal Raman and SERS spectra of the LSCF pellets annealed in ambient air, 10% H_2O, 5% CO_2, and 3% H_2O with Cr. The normal Raman spectra of these samples still showed no distinction. However, after SERS activation, the signals from the surface contaminations are observed. The Cr poisoned samples showed significant contamination peaks. The peaks around 810 and 850 cm^{-1} are associated with the $SrCrO_4$ phase, while the 340 cm^{-1} peak can be related to Cr_2O_3 [37]. The peaks at 930 and 980 emerged after firing the LSCF pellets in H_2O, CO_2, and ambient air. Such

peaks were observed in $LaFeO_3$ powders, which would be largely eliminated after A-site doping [38].

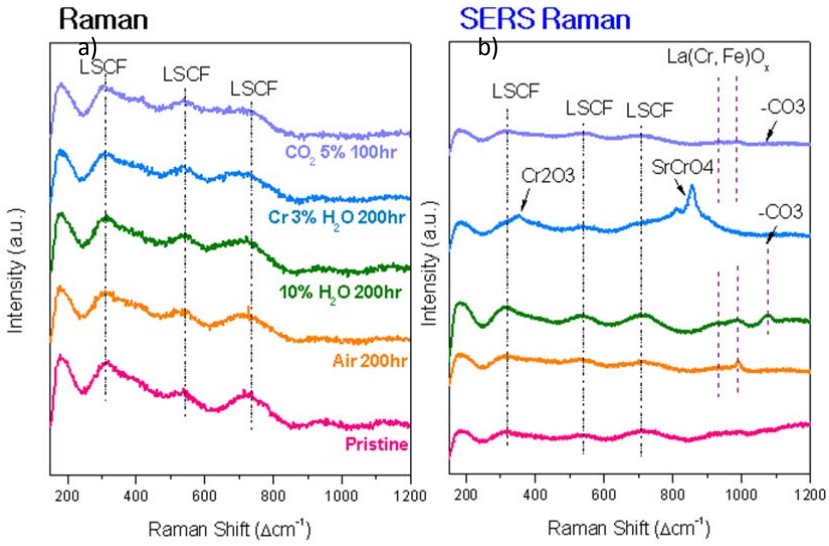

Figure 19 Raman and SERS analysis of LSCF pellets annealed under environments with higher concentration of contaminations. a) Normal Raman spectra of LSCF pellets and b) SERS spectra.

From the aforementioned SERS analysis, it may be concluded that H_2O and CO_2 could influence the segregation of SrO. Since SrO itself possesses no active Raman modes, the segregation is identified indirectly. LSCF is based on the $LaFeO_3$ perovskite structure. At low Sr content, $LaFeO_3$ assumes an orthorhombic structure (**Pbmn** space group), while at high Sr content, it transforms to a rhombohedral structure (**R3c**), according to the XRD analysis of the bulk samples by Tai et al. [39]. The main peaks of LSCF (310, 540, and 720 cm^{-1}) are believed to be associated with the R3c structure, since the pristine LSCF with and without SERS both possess these peaks. The emerging of small peaks around 500-600 cm^{-1} and the appearance of 930 and 980 cm^{-1} peaks suggest that orthorhombic phases are formed after annealing in H_2O and CO_2. The formation of the orthorhombic phase only occurs in LSCF when Sr is removed from the perovskite lattice, which signifies SrO segregation [38].

The SERS study also indicated that the contamination of Cr species presents in two forms, Cr_2O_3 and $SrCrO_4$. The Cr species in the alloy can sublimate into the

atmosphere and subsequently deposit on the LSCF surface in the form of Cr_2O_3. The Cr_2O_3 can then react with segregated SrO to form $SrCrO_4$. Cr poisoning can occur through a solid state diffusion path when LSCF is in direct contact with Cr alloy as well as a gas diffusion path. To compare the effects of solid state diffusion and gas phase diffusion, LSCF thin film electrodes were tested with and without direct contact to the Cr alloy interconnect, as shown in **Figure 20**. The LSCF thin film was fabricated by RF magnetron sputtering, and a special cell fixture was devised. One cell has the LSCF thin film electrode in contact with the Cr alloy, while the other has the Cr alloy in contact with the counter electrode. Both cells are tested under cathodic bias of 1.5V at 750°C for 100 h. Air humidified with 10% H_2O using a humidifier set at 43°C was used as the atmosphere.

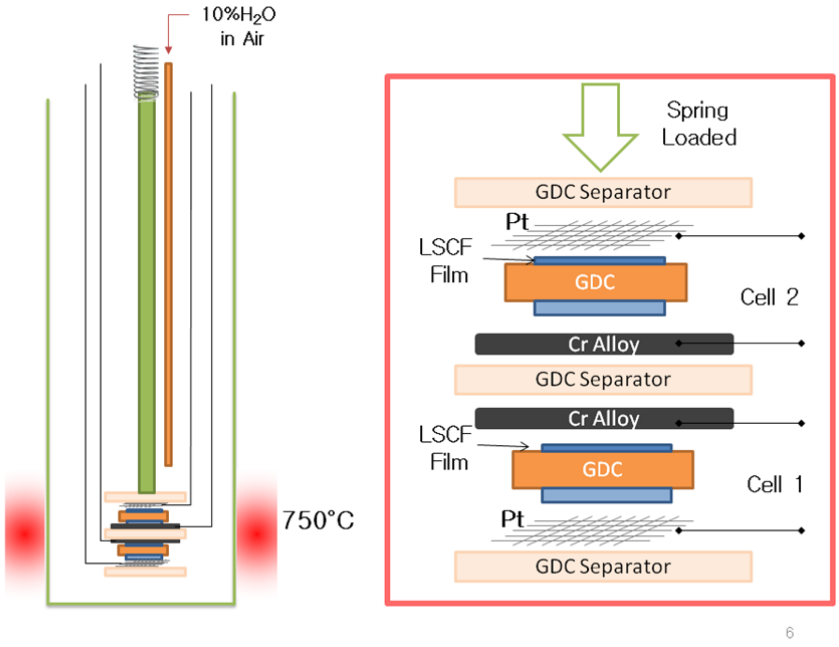

Figure 20 Testing apparatus for the Cr poisoning on the LSCF thin film electrodes. The LSCF thin film in Cell 1 is in direct contact with the Cr alloy, while that in Cell 2 is not in direct contact.

Surface enhanced Raman spectroscopy was conducted on LSCF thin film electrodes *post mortem*. After sputtering the samples with Ag nanoparticles, Raman spectra were collected across the GDC-LSCF boundaries, as shown in **Figure 21**. On both samples,

the spectra collected on LSCF film showed a prominent feature at 700 cm^{-1}, corresponding to one of the E_g modes. The electrode in direct contact with Cr alloy showed multiple bands between 800 cm^{-1} and 900 cm^{-1}, suggesting the deposition of $SrCrO_4$ [40]. Meanwhile, the LSCF electrode not in contact with Cr alloy showed no significant features between 800 cm^{-1} and 900 cm^{-1}, indicating that the $SrCrO_4$ deposition through gas diffusion is much less significant. This conclusion is consistent with the electrochemical experiments, in which the LSCF electrode in direct contact with Cr alloy showed more severe degradation. We also noticed that in the LSCF electrode in contact with the Cr alloy, the features of $SrCrO_4$ are more prominent on the LSCF-GDC boundary, which suggest a preferential spatial deposition of $SrCrO_4$.

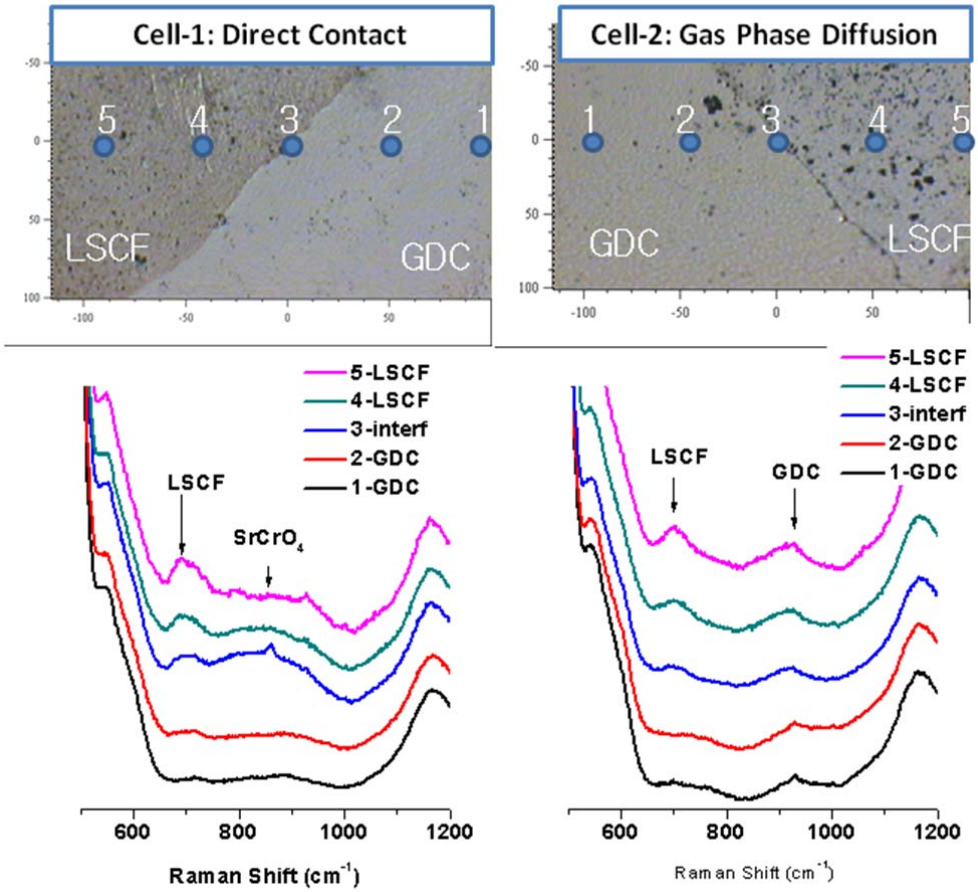

Figure 21 Surface enhanced Raman spectroscopy on the boundaries between the LSCF thin film electrodes and GDC substrates. Cell 1 is in direct contact with the Cr containing alloy while cell 2 is not.

The deposition of $SrCrO_4$ on the LSCF boundary offers new insight into the Cr poisoning mechanism of LSCF electrodes: $SrCrO_4$ could block the active sites for oxygen reduction on the triple phase boundary. To validate this hypothesis, patterned LSCF electrodes were fabricated and tested in an *in situ* Raman chamber at 550°C with 3% H_2O carried in air, as shown in **Figure 22a**. The *in situ* Raman on the patterned LSCF electrodes showed no significant features related to Cr deposition. However, evidence of Cr poisoning manifested after SERS agents are applied. SERS mapping was conducted over a region covering one LSCF electrode with electrical bias and one without electrical bias. The intensities of the peaks related to GDC (465 cm^{-1}) and LSCF (670 cm^{-1}) are consistent with the locations of the patterned LSCF electrodes. The peak at 860 cm^{-1}, which corresponds to the deposition of $SrCrO_4$, is concentrated on the LSCF-GDC interfaces. In contrast, previous research of Cr poisoning of SOFC cathodes indicated that $SrCrO_4$ formed on the surface of LSCF rather than at the LSCF-GDC boundary [12, 41]. This inconsistency necessitates further research. The electrical bias has no preferential effect on the formation of $SrCrO_4$, which agrees with the previous report [41].

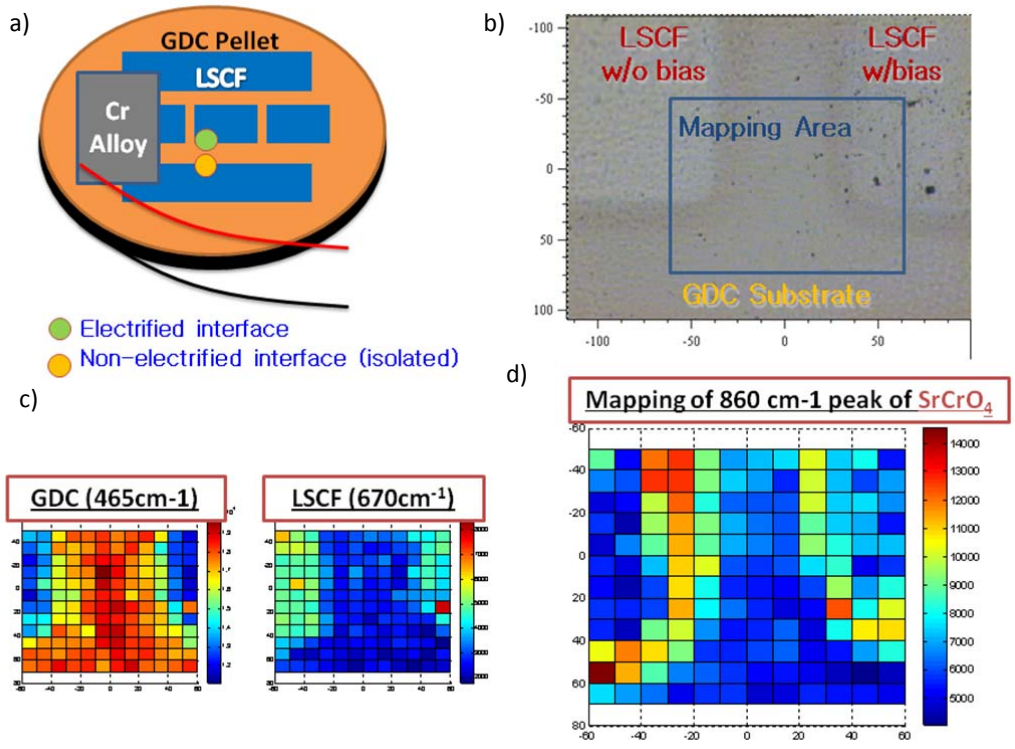

Figure 22 The SERS mapping of the LSCF electrodes after Cr poisoning. The $SrCrO_4$ peak at 890 cm^{-1} concentrates on the LSCF-GDC boundaries.

In summary, Raman spectroscopy is a unique tool to identify the surface species on the LSCF electrodes. With the SERS effect provided by sputtered Ag nanoparticles, the sensitivity towards species with low concentrations improves significantly. SERS makes many surface species related to the LSCF degradation detectable. The preliminary results presented herein indicates that the SrO segregation occurs after long-term annealing, $SrCrO_4$ forms in the presence of direct Cr alloy contact, and $SrCrO_4$ preferentially deposits on LSCF-GDC boundary.

Synchrotron-based in situ X-ray photoelectron spectroscopy (XPS) study of the LSCF exposure to contaminants

Synchrotron-based XPS was performed to study the effects of CO_2 and H_2O exposure on the LSCF chemical and electronic state at the surface. Synchrotron-based soft x-ray photoelectron spectroscopy (XPS) was performed at Beamline U12A of the NSLS at BNL using photon energy of 600 eV for high surface specificity. The LSCF thin film symmetrical cathode sample was mounted on a tungsten wire heating stage

attached to the manipulator arm. Photoelectron spectra were collected at 25°C, 400°C, and 750°C prior to a cycle of backfilling to 1.0 x 10-7 torr with CO_2, H_2O, and equal mixtures thereof, and evacuating to UHV at that temperature. After heating and gas cycling at 750°C, the sample was cooled to 25°C in an equal mixture of H_2O and CO_2 at a roughly constant partial pressure. After evacuating the chamber to UHV conditions, the photoemission spectra were collected again. The unique ability of the synchrotron was to use lower energy photons to constrain the information depth to be more surface sensitive and to use a main chamber that was specially designed to perform an in situ high temperature gas exposure on the samples. To prepare an ideal cell for characterization, we began with a single crystal of YSZ. To simplify the experiment, we designed a symmetrical cathode cell with a porous LSCF counter electrode with SDC buffer layer and an LSCF thin film working electrode, which would be open to gas contaminants and x-rays for characterization. For the LSCF thin film cathode, we desired a cathode with model geometry so that the interaction phenomenon would be limited to a controlled region of study. Thus, we fabricated a 200 nm LSCF thin film on YSZ single crystal by two stages of sputtering, with a heating stage at 500°C for 1 h in air in between to relieve mechanical stress and reconstruct the surface before the second stage of sputtering. A final annealing stage at 800°C for 1 h in air was used to finish the synthesis. Two samples were studied for the series of temperature and gas exposures. The first sample, termed “Sample 1”, was the as-prepared LSCF thin film. The second sample, termed “Sample 2”, was a similarly prepared LSCF thin film that was first annealed in a 10% H_2O atmosphere at 750 ^oC for 60 hours, to identify if there were any long-term effects.

The XPS results are summarized in **Figure 23** and **Figure 24**. The XPS peak fitting results have helped clarify two initial questions in the experiments. The first, whether the 60 h long term anneal in 10% H_2O environment had an effect on the chemical state of particular cations, was evidenced in the behavior of the La 4d photoemission measured at 25°C before and after the series of exposures. Whereas the as-prepared LSCF thin film began with a relatively higher amount of the pre-emission species, according to area ratios, and ended with a relatively lower amount, the water annealed

LSCF thin film exhibited the opposite trend. Second, the transient nature of surface species was demonstrated by comparing the low and high temperature exposures. In the as-prepared sample, there was little change in the relative area ratios by peak. This indicates that either the intermediate exposures created only transient surface species which were eventually removed by the high temperature state or that the intermediate exposures had no effect on the surface La. In contrast, the water annealed sample showed significant change in the area ratios at high temperature after intermediate exposures, indicating that the water annealing affected the transiency of the surface species. Additionally, it is important to consider that La is typically considered to be a relatively stable cation that serves primarily a stability purpose in the crystal structure, whereas the dopants and transition metals serve the catalytic and transport purposes. However, this XPS data provides some grounding to the contrary.

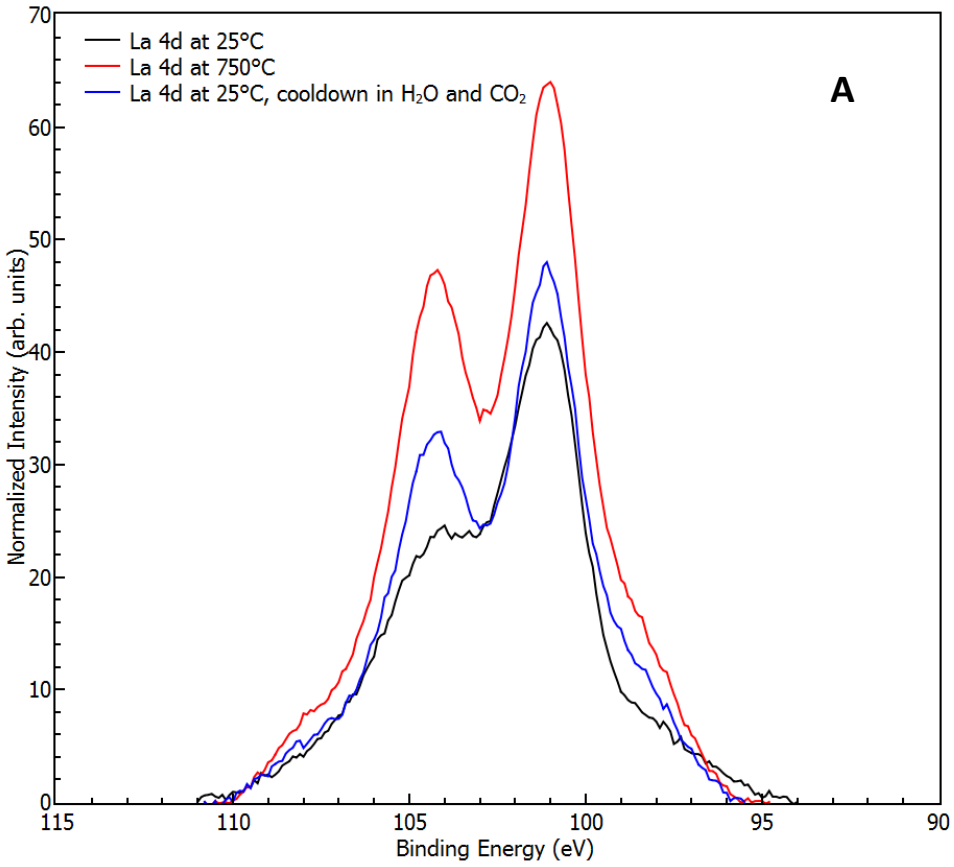

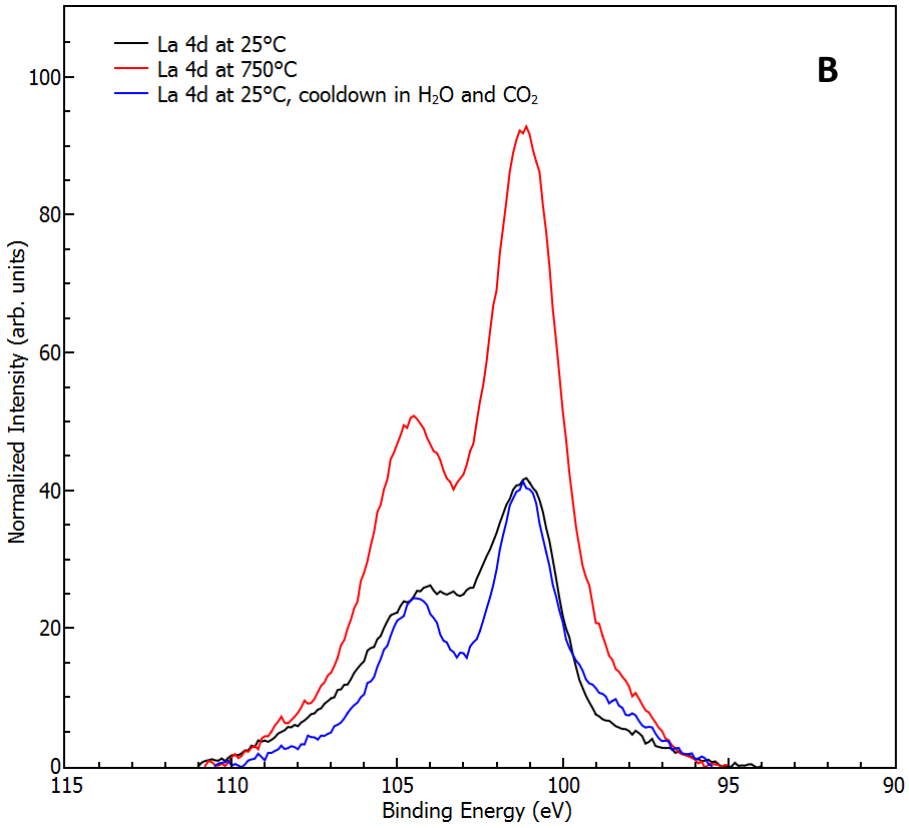

Figure 23 The La 4d photoemission, after background removal and intensity normalization, of (A) Sample 1, as-prepared LSCF thin film, and (B) Sample 2, the water annealed LSCF thin film.

These *operando* experiments provided useful insight into the different influences of CO_2 and H_2O on the Fe and Co cations of the LSCF thin film cathode. It was found that greater increases in polarization resistance at lower temperatures correlated to greater oxidative shifts in the edge energy of Fe and Co. The XANES indicated that CO_2 had slightly oxidizing effects while H_2O had a neutral effect on Co and slightly reducing effect on Fe at 700°C. However, the FT EXAFS showed that Co local structure underwent significant deformation in the first coordination shell, resulting in an elongated bond length. Meanwhile, the Fe local structure appeared to be relatively stable and only increased in the magnitude of the first coordination shell peak, indicating filling of oxygen vacancies by lattice oxygen, carbonate, or hydroxide ligands. Synchrotron-based XPS complemented the *operando* XAS by providing

information about the carbonate species, photoemissions from presumably new Co-containing phases, and different bonds based on oxygen photoemissions. The combination of these techniques, along with EIS and *in situ* XAS, enabled us to speculate that the Co cation is particularly susceptible deformation in the local structure and phase segregation over time, and, thus, it should be the focus of future investigations and rational materials design.

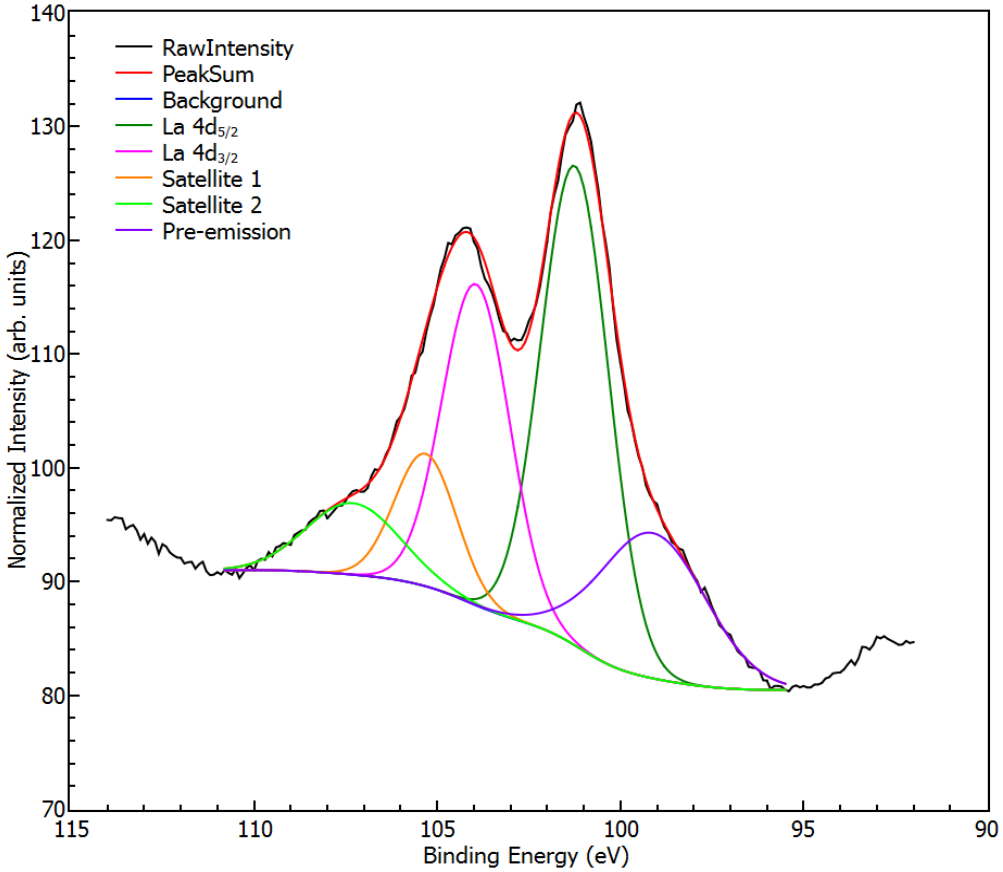

Figure 24 An example of the peak fitting results for the as-prepared LSCF thin film after cool down.

2.4 Proposed mechanism of the Rp or stability change when the LSCF is exposed to H_2O, CO_2 and Cr containing materials.

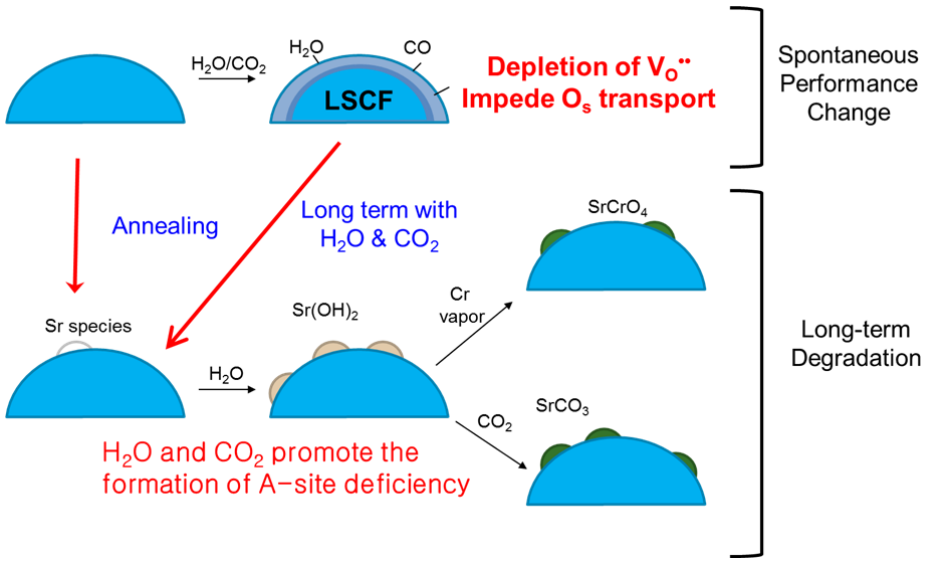

Figure 25 Possible degradation mechanisms of LSCF cathode in contaminants

Based on the information we have collected from electrochemical measurements, Raman analysis and synchrotron-based X-ray experiments, we formulated some preliminary hypotheses about how H_2O and CO_2 affect the performance of the LSCF cathode. Here is a brief summary of our hypotheses (**Figure 25**):

H_2O or CO_2 molecules may absorb on the surface of the LSCF, which is more favorable at low temperatures while the total adsorption capacity of the LSCF cathode surface is independent of the temperature. The adsorbed species may bond to Co and Fe, and thus affect the valence of Co and Fe (especially Co). The bonding of H_2O and CO_2 with Co in the LSCF cathode may reduce the surface oxygen vacancy concentration, and also impede the transport of oxygen species from the adsorption/dissociation sites to other active sites. These might be the main reasons for the observed reversible change in performance. The adsorbed species may react with segregated/enriched Sr to form hydroxide and then carbonate. At the same time, the carbonate may be more stable thermodynamically so that segregation is exacerbated at the presence of H_2O and CO_2. This could be the main reason for long term degradation. The degradation in performance is accelerated by Cr-poisoning due to the presence of Cr-containing materials in the testing apparatus. Our results indicated that the presence of H_2O significantly exacerbated the degradation rate of the LSCF cathode in direct contact with a Cr-alloy, which may be associated with the following

two causes: a) both H_2O and CO_2 promote the formation of A-site deficiency which is very likely to accelerate the enrichment of Sr in LSCF (intrinsic degradation mechanism); b) the increased formation of Cr-containing surface species (e.g. $SrCrO_4$) (extrinsic degradation mechanism).

2.5 Exploration of promising catalysts, which can enhance the performance and durability of LSCF cathode

Properties for material candidate with tolerance against H_2O, CO_2 or Cr contaminant:

Based on our proposed mechanisms about the effect of H_2O and CO_2 on performance of the LSCF cathodes at the early stage, the most effective catalyst should possess the following properties in comparison with the LSCF:

a) Weaker adsorption capability for H_2O and/or CO_2 both physically and chemically;
b) More robust and stable local structure when bonded with H_2O and/or CO_2;
c) Compatible performance, or even better electrocatalytic activity than the LSCF;
d) No negative effect on the cathode durability.

Mitigation strategies:

To develop the conformal catalyst coatings, which can cover the whole surface of the LSCF cathode using the perovskite-related type materials, a well-designed infiltration process can introduce a thin film coating on the surface of the LSCF cathode (**Figure 26**).

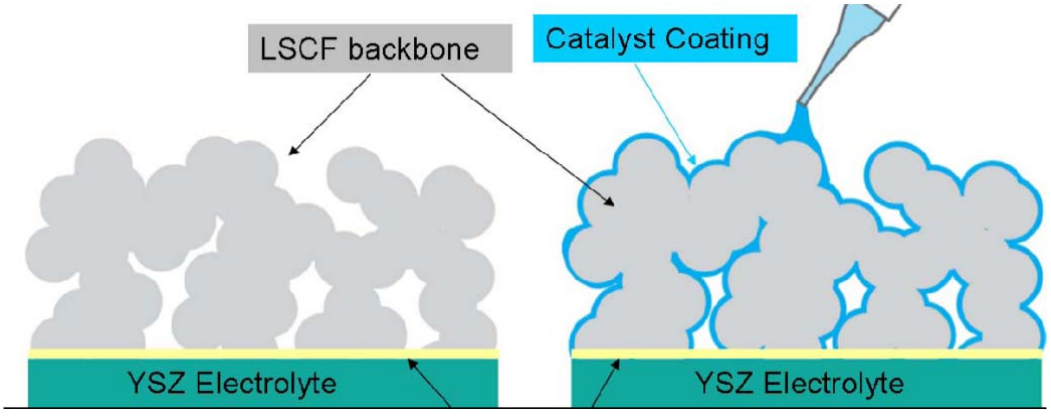

Figure 26 A schematic of a new catalyst coating on the surface of the LSCF cathodethrough infiltration.

Preliminarily, new catalyst coatings, such as $Pr_{0.9}MnO_{3-\delta}$ (PM), $La_{0.72}Sr_{0.18}MnO_{3-\delta}$ (LSM), and $Pr_2Ni_{1-x}Mn_xO_{4-\delta}$ (PNM), were used to modify the surface of the LSCF cathode, and preliminary results showed that the order of resistance to H_2O and CO_2 poisoning is PM > LSM > LSCF > PNM while the order of electrocatalytic activity is PNM > LSM > PM under OCV condition. These results show that our proposed materials are effective.

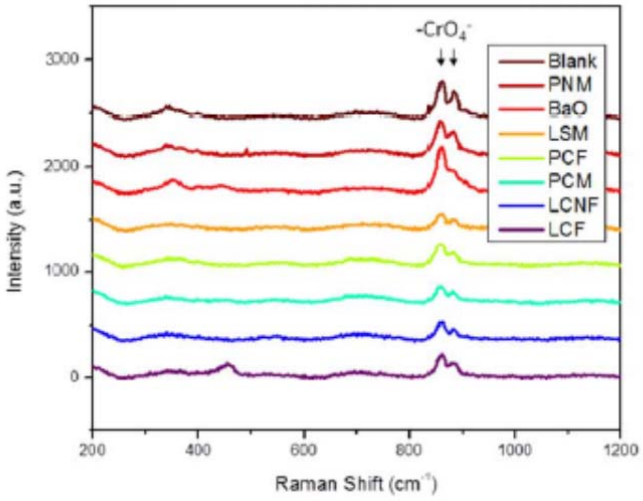

Figure 27 Raman spectra collected on LSCF electrode with different materials after annealing with Crofer. Annealing conditions: 750 ^oC for 75 h with air containing 3% H_2O

In order to identify effective catalysts against Cr-poisoning, Raman spectroscopy was used to evaluate the reactivity between Cr vapor and various LSCF porous electrodes modified with different surface catalysts. The Cr poisoning process was simulated by annealing the porous electrode with Cr alloy at 750 ^oC in the presence of 3% H_2O. Electrodes were stacked in contact with the Crofer 22 APU foils. In total, 25 random locations were inspected with Raman spectroscopy on each sample, in order to gain statistical reliability and to observe the Cr distribution on the cathode surface. A 514 nm laser was used to excite Raman scattering. All spectra were normalized by the leading edge of the Raman spectra (170 cm^{-1}) and the fluorescence was removed by background subtraction. The ensemble-averaged Raman spectra of different

modifications after Cr treatment are presented in **Figure 27**. Two peaks at 860 cm^{-1} and 880 cm-1 can be associated with the formation of -CrO^{4-} phases. While different modifications resulted in variations of the intensity of the -CrO^{4-} peaks, it is hard to derive a conclusion about each modification's resistance to Cr poisoning.

In order to gain more insight to the Cr resistance capability of different materials, statistical analyses were performed on the 25 spectra collected on each sample. Shown in **Figure 28** are the cumulative probability plots of the intensity of 860 cm^{-1} peak of all samples. While in all samples the intensity of the -CrO_4^- peak showed a wide distribution, on certain modification materials (e.g. LSM, LCF, PCM, and LCNF), low intensity values show larger probability. This indicates a larger area on such samples being resistant to Cr poisoning. Since the Cr poisoning test adopted in this study is an aggressive process, and the coating on porous may not be uniform, a larger area containing lower concentration of -CrO_4^- phase might be the only feasible indication of Cr resistance. Further statistical analysis was conducted to compare the Cr resistance of different modification materials directly. The average and median peak intensity of the 860 cm^{-1} peak of different electrode modifications are shown in **Figure 29**. The median value of the intensity is a descriptor of the statistical effect of Cr resistance of different modification materials. Compared with blank LSCF porous electrode, the electrodes modified with LCF, LCNF, PCM, and LSM showed prominent reduction of the -CrO_4^- phase on most of their surfaces, suggesting a certain degree of resistance to Cr poisoning.

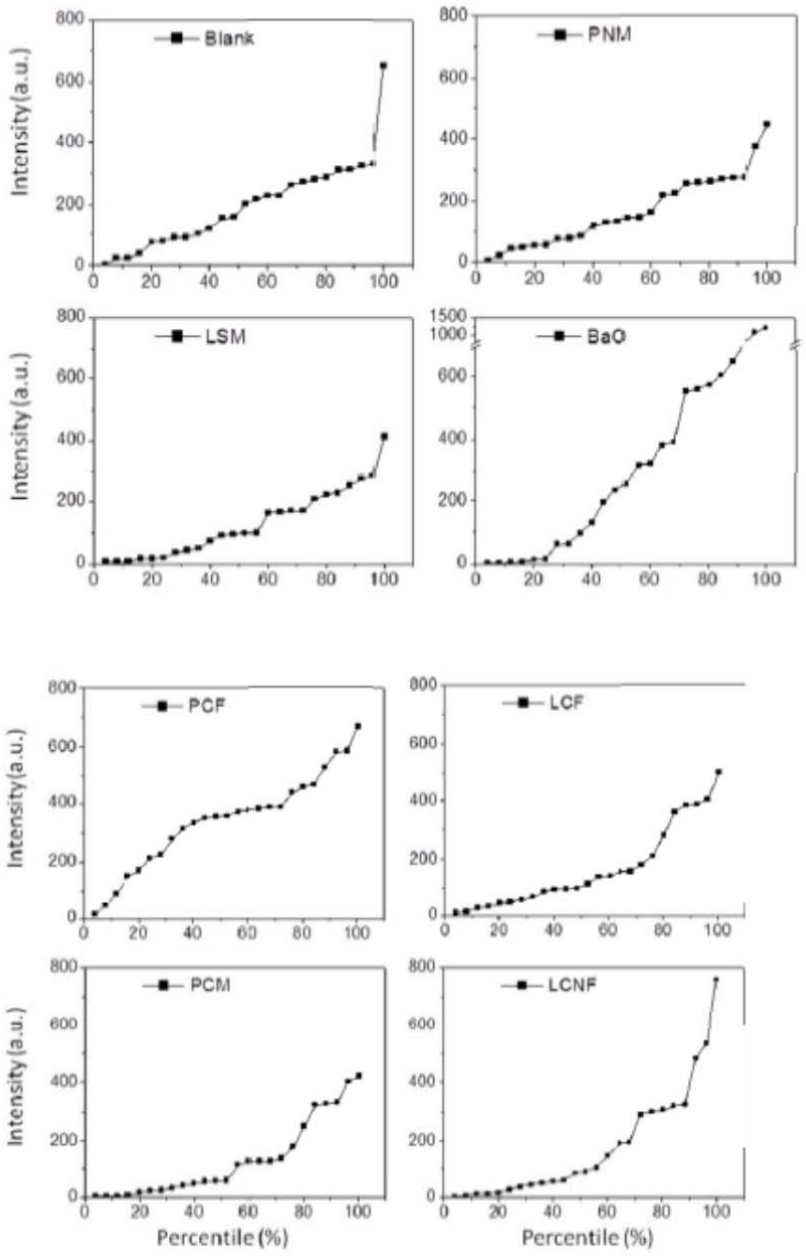

Figure 28 Cumulative probability plot of the 860 cm^{-1} peak intensity of Raman spectra collected from catalyst-coated LSCF

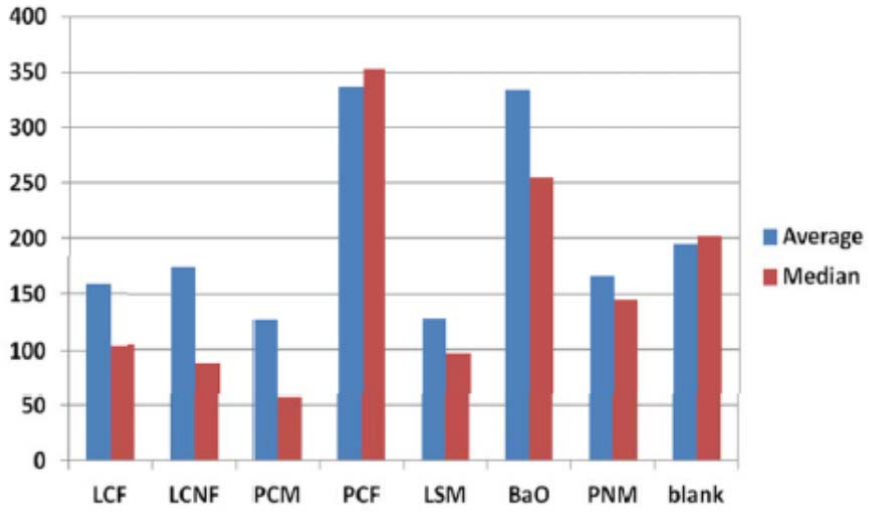

Figure 29 Average and median peak intensity of the 860 cm-1 band from LSCF and catalyst coated LSCF after Cr poisoning testing

Raman measurements for catalyst-infiltrated LSCF cathodes chemically exposed to contaminants as a fast materials screening procedure

In order to identify effective catalysts against Cr poisoning, Raman spectroscopy was used to evaluate the reactivity of Cr and LSCF electrodes with different surface catalysts as we did in previous reports. In our previous report, we studied the effects of Cr poisoning on different types of catalyst coating by directly annealing the Cr foils and cathodes together. By comparing the intensities of Raman bands of Cr related species, the resistance of different catalyst coatings was examined. The electrodes modified with LCF, LCNF, PCM, and LSM showed prominent resistance to Cr poisoning.

It is well known that direct contact of the SOFC cathode and the Cr foil or alloy is a primary reason for Cr poisoning. However, under high temperature conditions, the Cr vapor could also diffuse to the cathode surface, forming Cr related species and impeding the oxygen reduction reactions. In order to gain more insight of the Cr poisoning, we conducted the experiment shown in **Figure 30**. The LSCF cathodes with different catalyst coating were covered by semi-circle-shaped Cr foil. The cathode part in direct contact with the Cr suffered from direct migration of Cr. At the

same time, the Cr vapor will diffuse to the other side of cathode, forming Cr related species especially near the boundary of Cr contacted cathode. After the Cr foil was removed, Raman spectra were taken at the region without direct Cr contact (100μm away from boundary). The same Raman spectra acquisition was also conducted in the area with direct Cr contact as a comparison (**Figure 30**). An argon-ion laser with 514 nm wavelength was applied as the excitation laser and a 20x objective was used to focus the laser and collect Raman spectra.

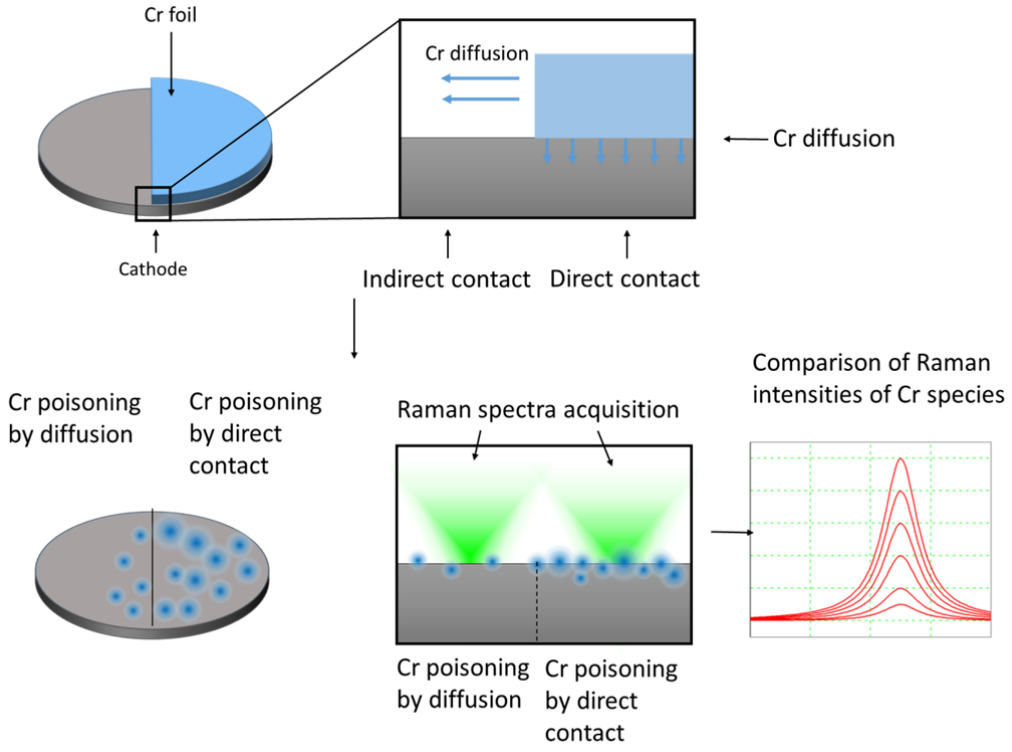

Figure 30 Schematic of the sample preparation process and Raman spectra acquisition of Cr poisoning study. The cathode was covered by a semi-circle of Cr foil and then annealed at 750 ^{o}C in the presence of 3% H_2O. The effects of Cr poisoning by direct Cr contact and Cr gas diffusion are schematically shown. Raman spectra were taken at the region without direct Cr contact (100μm away from boundary) and the region with direct Cr contact for comparison.

The ensemble-averaged Raman spectra of different catalyst coating on LSCF substrate after Cr treatments (direct and indirect contact) are presented in **Figure 31**. After the exposure to Cr (whether by direct contact or vapor diffusion), a few bands were detected as a results of Cr poisoning. As mentioned in our previous studies, the Raman bands between 800 cm^{-1} and 950 cm^{-1} could be attributed to various Cr (VI) species which are the primary species lead to Cr poisoning, such as $SrCrO_4$. The intensities of such bands could be considered as a semi-quantitative evaluation of Cr resistance. Higher band intensities correspond to poor resistance. For comparison purposes, the intensities of different Raman spectra are presented in the same scale. As evident in **Figure 31**, the intensities of Cr species caused by direct Cr contact (black spectra) are significantly higher than the intensities of Cr species due to Cr vapor diffusion (red spectra). This phenomenon is expected since direct Cr contact should lead to more serious Cr poisoning effects.

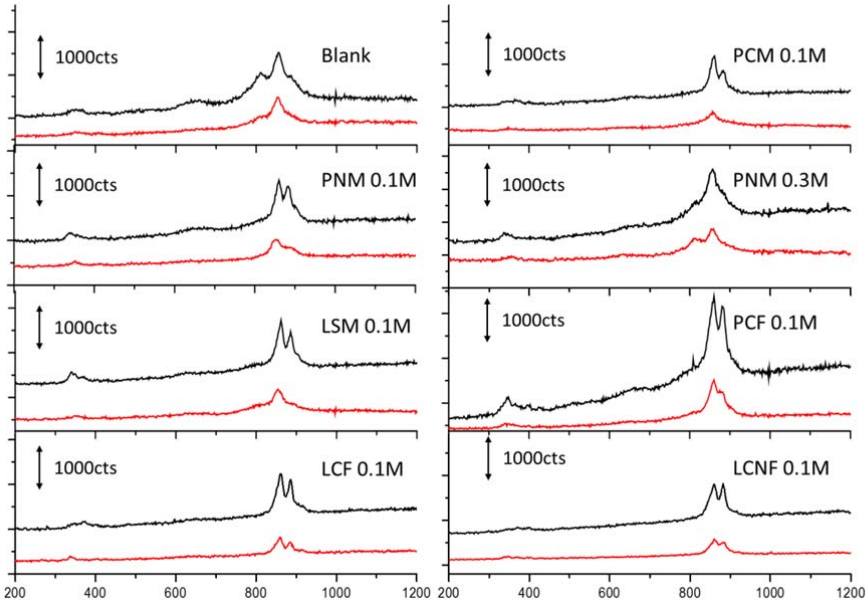

Figure 31 The Raman spectra of LSCF cathodes with various catalyst coatings: the spectra collected on the area of direct Cr contact (black); the spectra collected on the area of without Cr contact (red).

Further statistical analysis was conducted to compare the Cr resistance of different catalyst modifications. The integrated intensities of Raman bands between 800 cm^{-1} to 950 cm^{-1} are shown in **Figure 32**. The degree of Cr poisoning caused by Cr vapor

diffusion is substantially lower than direct Cr contact. All modified cathodes exhibited some degree of Cr resistance compared to the blank LSCF (except PCF), which basically agree with the conclusions of our previous report. The cathode modified by PCM exhibited the best Cr resistance in terms of direct Cr contact and vapor diffusion.

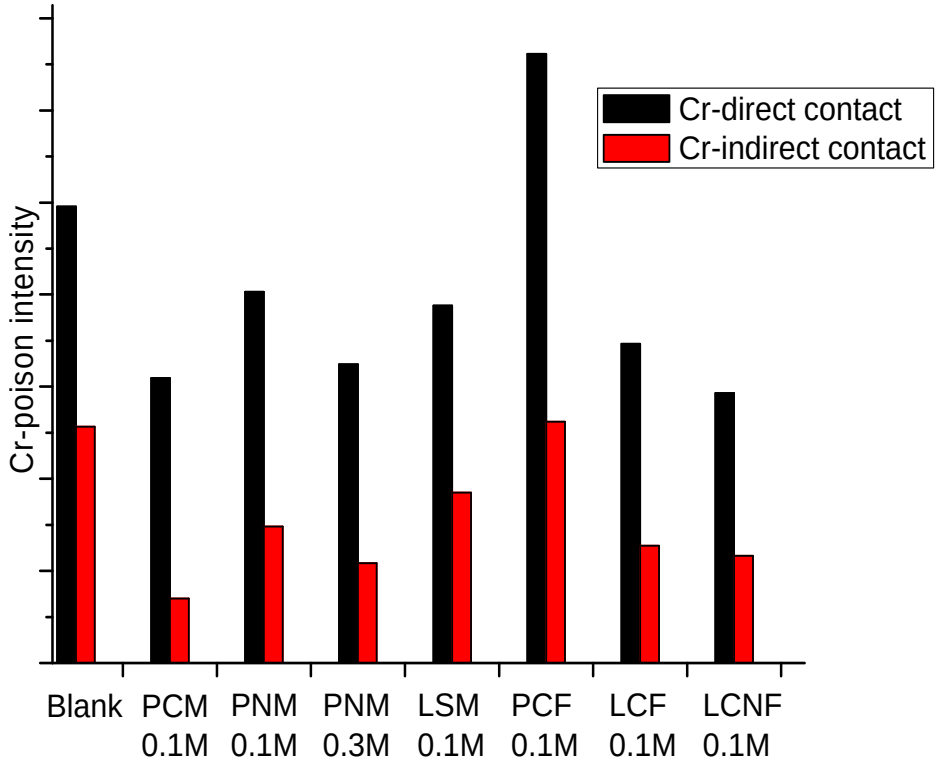

Figure 32 The Raman peak intensity of Cr related species collected on Cr direct contact area (black) and Cr indirect contact area (red) of LSCF cathode with various catalyst coating.

Our materials screening has demonstrated that certain catalyst coatings are effective for contaminant tolerance. In the present study, we applied a catalyst coating to LSCF based symmetrical cells and electrochemically demonstrated its effectiveness. We first employed the best catalyst discovered thus far, which is a mixture of PrO_x and single perovskite $PrNi_{0.5}Mn_{0.5}O_{3-\delta}$. The reason this mixture was chosen is that the PNM coating significantly enhances both the electrocatalytic activity and durability

under normal conditions (without contamination). It is assumed that it would remain the best catalyst, as long as the PNM coating can demonstrate contaminant tolerance. The detailed experiment is described as follows: the nitrate precursor with proper surfactants and complexing agents was infiltrated into LSCF-based symmetrical cells. After drying, the nitrate was decomposed *in situ* to form the desired phase when the cell was set up in the testing fixture and ramped up to 750°C, which is the testing temperature. We applied constant voltage to collect the current and then calculated the overpotential. As shown in **Figure 33**, the infiltrated and blank LSCF cathode exhibited the different degradation rates with 3% H_2O+1% CO_2 in the presence of Cr alloy. This suggests that the PNM coating has remarkable contamination tolerance. In the future, we will infiltrate it into the full cell for more comprehensive investigation and demonstration.

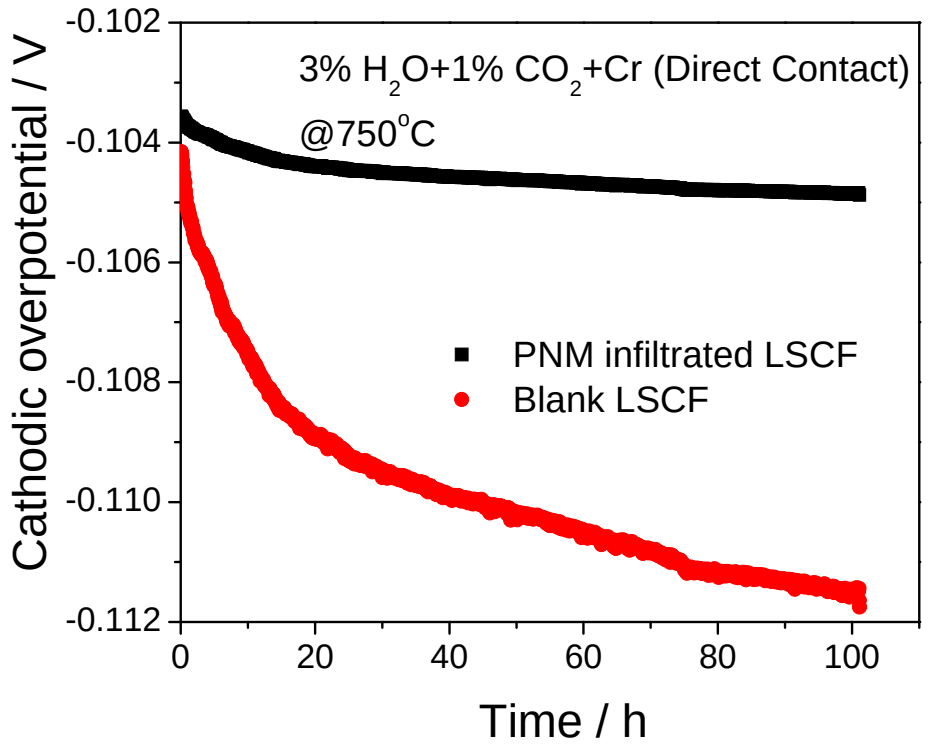

Figure 33 Cathodic overpotential of the PNM infiltrated LSCF and blank LSCF cathode in contact with Cr materials at 3% H_2O+1% CO_2, measured at 750°C at a constant voltage of 0.40 V and 0.25 V at 750°C, respectively.

2.6 Performance evaluation of single cells with blank LSCF and catalyst coated LSCF cathodes in ROC conditions

We have evaluated the performance of single cells with blank LSCF under different contamination conditions. The performance (IVP curve) and durability (at voltage of 0.7V) were shown in **Figure 34**. H_2O or CO_2 molecules may absorb on the surface of the LSCF. Adsorbed H_2O and CO_2 may react with segregated Sr (or Co) to form hydroxide and then carbonate. Since carbonate may be more stable thermodynamically at operating temperatures, Sr (or Co) segregation is further exacerbated in the presence of H_2O and CO_2. In direct Cr contact, H_2O and CO_2 significantly exacerbated the degradation rate of the LSCF cathode. Both H_2O and CO_2 promote the formation of A-site deficiency, accelerating the enrichment of Sr in LSCF (intrinsic degradation mechanism). The increased formation of Cr-containing surface species (e.g. $SrCrO_4$) (extrinsic degradation mechanism).

Further, we have selected the best catalyst, PNM, as the coating layer on LSCF surface, according to our previous selection (**Figure 35**). With infiltration of 5 μL 0.1 M catalyst solution on LSCF, the initial cell performances (P_{max}) have been enhanced compared with the cell with blank LSCF cathode without catalyst coating. The performance enhancement could be attributed to the cathode since the anode and electrolyte were kept the same, indicating that thin catalyst coatings could alleviate the degradation of cathode. For example, when exposed to the contamination (3% H_2O, 5% CO_2 and direct contact with Crofer), the cell with blank LSCF can only deliver a P_{max} of ~0.34 Wcm^{-2}. However, the cell with PNM coated LSCF can deliver a P_{max} of ~ 0.62 Wcm^{-2}. Figure 31b shows the long-term stability of single cells with blank LSCF, PrO_x-coated LSCF, and PNM-coated LSCF cathodes with harsh contamination of 3% H_2O, 5% CO_2 and direct Crofer contact measured at 750 ^oC under contestant voltage of 0.7V. It can be clearly shown that the coatings could alleviate the degradation rate. Our best catalyst determined from symmetrical cell studies, PNM, shows the best tolerance.

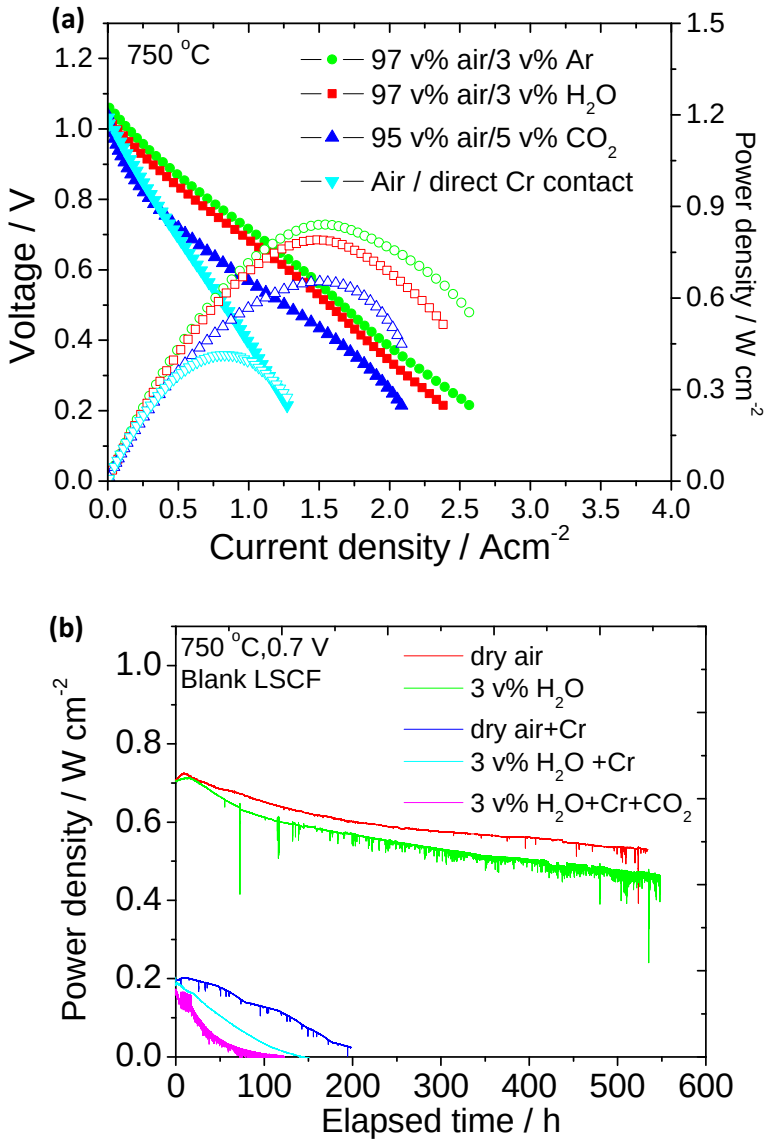

Figure 34 IVP curves (a) and long-term stability test (b) of single cells with blank LSCF in different contamination conditions, measured at 750 °C when wet H_2 was used as fuel

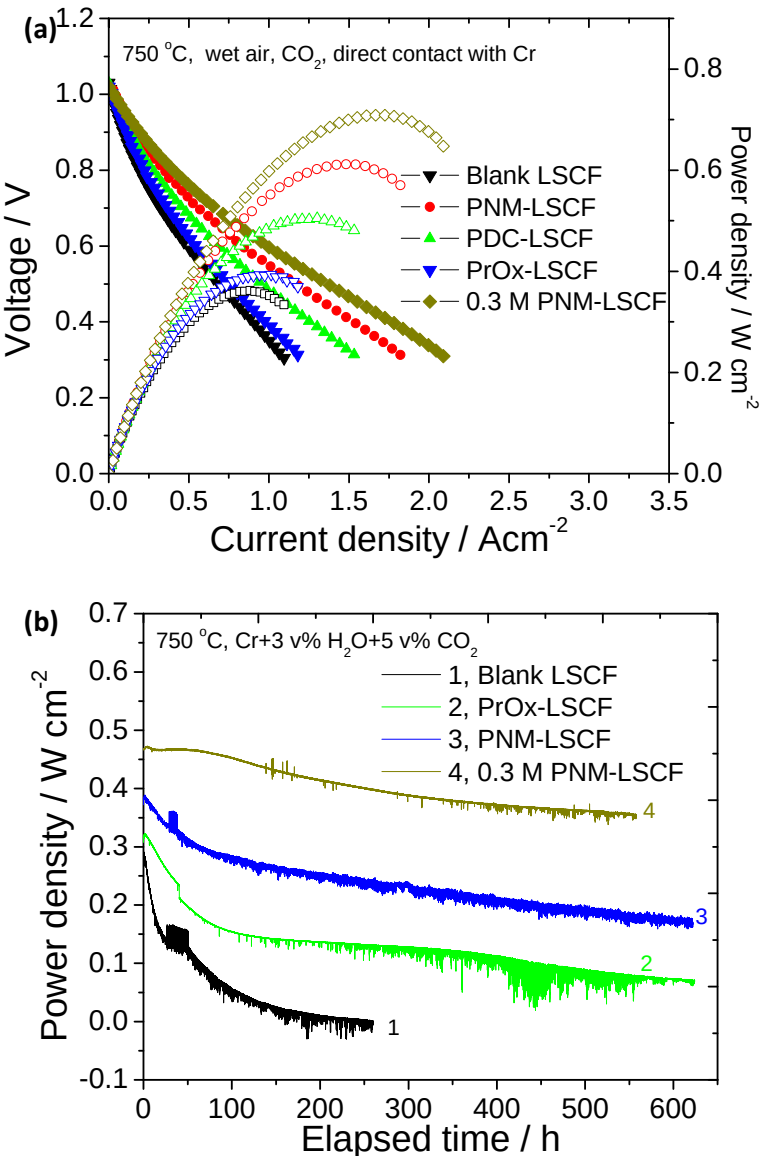

Figure 35 IVP curves (a) and long-term stability test (b) of single cells with PNM-coated LSCF in different contamination conditions, measured at 750 °C when wet H_2 was used as fuel

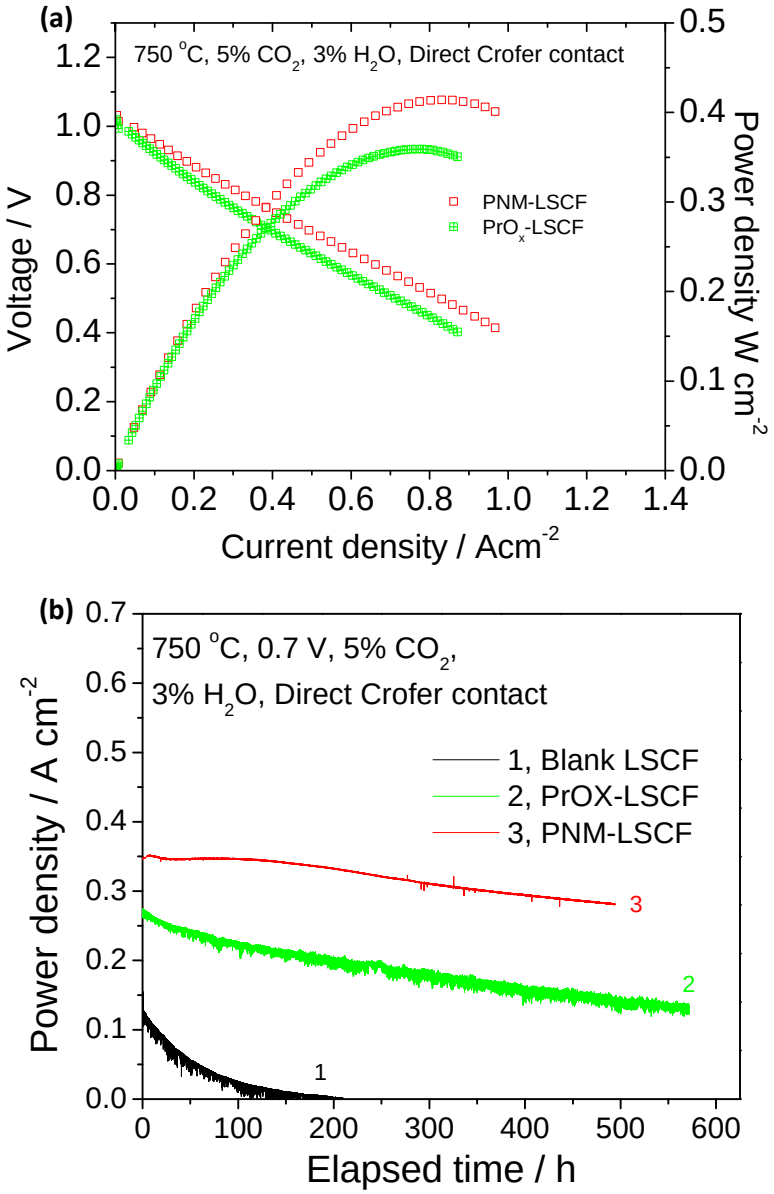

Figure 36 Typical *I-V-P* curves (a) and durability test (b) for commercial cells with PNM- and PrO_x-coated LSCF cathodes. The catalyst was introduced by a solution infiltration process (derived from 5 µL 0.3 M nitrate solution). All cells were operated at a constant cell voltage of 0.7 V at 750 °C.

Also, we also evaluated the performance of commercial anode-supported cells with catalyst coated LSCF under contamination conditions (5% CO_2, 3% H_2O and direct Crofer contact) (**Figure 36**). The commercial cells were purchased from Materials and System Research, Inc (MSRI). The configuration of the commercial cells as well as

the thickness were kept consistent with our previous home-made cells (anode NiO-YSZ (800 μm), NiO-YSZ functional layer (15 μm), YSZ (15 μm), SDC buffer layer (2-4 μm), LSCF (50 μm). Still, it can be clearly seen that cathodes with the PNM and the PrO_x catalyst coating show much lower degradation rate, confirming the effectiveness of the catalysts against contaminants (CO_2, H_2O, and Cr) poisoning.

5. CONCLUTIONS

We have successfully characterized the electrochemical behavior of LSCF cathodes under realistic operating conditions (ROC) with different types of contaminants (e.g., H_2O, CO_2, and Cr). We have also unraveled the degradation mechanism of LSCF cathodes when exposed to different types of contaminants using *in situ* and *ex situ* measurements performed on cells with specially-designed cathodes. Microstructural and compositional evolution of LSCF cathodes as well as the cathode/electrolyte interfaces under ROC has been evaluated. We have correlated the fuel cell performance instability and degradation with the microstructural and morphological evolution and surface chemistry change of the cathode under realistic operating conditions. We demonstrated that the activity and stability of LSCF cathodes under real operation conditions (with contaminates) can be enhanced by the introduction of a thin-film catalyst coating through a simple and cost-effective solution infiltration process. A surface enhanced Raman technique was developed and the signal enhancements were obtained for catalysts and LSCF films/interfaces on underlying GDC substrate, enabling us to capture the surface/interface information in perovskite-related cathodes. Electrochemical models for the design of test cells and understanding of mechanisms were developed for the exploration of fundamental properties of electrode materials. Raman spectroscopy (including SERS) and synchrotron-based x-ray analyses (e.g., XAS) are powerful techniques for probing electrode surfaces under various conditions. Together with the modeling and simulation tools developed earlier under this project, these characterization techniques helped us to unravel the mechanism of catalyst-infiltrated electrodes, thus providing scientific basis for rational design of more efficient cathode materials and structures. Based on the knowledge we gained from PNM infiltration, continuous thin films were developed to further improve the activity and stability of the LSCF cathodes. Microstructural examination of tested cells did not show visible differences between the blank and the catalyst-infiltrated electrodes. There was no significant change in

the morphology or microstructure of the PNM-coated LSCF cathodes due to the structural similarity of LSCF and PNM.

We also explored new catalyst materials and electrode structures to enhance the stability of the LSCF cathode under realistic operating conditions. We have validated the long term stability of PNM modified LSCF cathodes, which showed best ORR kinetics and durability in commercially available cells under realistic operating conditions. Further, the surface and interface of blank LSCF cathodes without surface modification and LSM-coated LSCF cathodes were systematically characterized before and after electrochemical testing using advanced microscopy and spectroscopy techniques.

Publications

1. Ze Liu, Mingfei Liu, Lei Yang, Meilin Liu*, LSM-Infiltrated LSCF cathodes for solid oxide fuel cells, Journal of Energy Chemistry, 22 (2013) 555-559.
2. Dong Ding, Mingfei Liu, Zhangbo Liu, Xiaxi Li, Kevin Blinn, Xingbao Zhu, Meilin Liu*, "Efficient Electro-Catalysts for Enhancing Surface Activity and Stability of SOFC Cathodes", Advanced Energy Materials , 2013, 3, 1149-1154.
3. Lynch, Matthew; Ding, Dong; Harris, William H.; Lombardo, Jeffrey J.; Nelson, George J.; Chiu, W. K. S.; and Liu, Meilin*, Flexible Multiphysics Simulation of Porous Electrodes: Conformal to 3D Reconstructed Microstructures, Nano Energy, 2, 105-115 (2013). [10.1016/j.nanoen.2012.08.002]
4. Dong Ding, Xiaxi Li, Samson Lai, Kirk Gerdes, and Meilin Liu, "Enhancing SOFC Cathode Performance by Surface Modification through Infiltration " Energy Environ. Sci, 2014, 7, 552-575. DOI: 10.1039/c3ee42926a.
5. Yu Chen, Yan Chen, Dong Ding, YongMan Choi, Lei Zhang, Ruiqiang Yan, Seonyong Yoo , Yong Ding, Qiyang Lu, Haibin Sun, Dongchang Chen, Bote Zhao, Renzong Hu, Hendrik Bluhm, Ethan J. Crumlin, Bilge Yildiz, and Meilin Liu, A catalytically-active and durable cathode for solid oxide fuel cells, to be submitted.
6. Yu Chen, Dong Ding, Dongchang Chen, Ruiqiang Yan, Meilin Liu, An efficient, high-performance, and robust cathode for solid oxide fuel cells, to be submitted
7. Yu Chen, Dong Ding, Dongchang Chen, Seonyoung Yoo, Haibin Sun, Ruiqiang Yan, Meilin Liu, A CO_2/H_2O tolerant cathode for solid oxide fuel cell, to be submitted.

References:

[1] N.Q. Minh, J Am Ceram Soc, 76 (1993) 563-588.
[2] B.C.H. Steele, A. Heinzel, Nature, 414 (2001) 345-352.
[3] S.C. Singhal, Solid State Ionics, 152 (2002) 405-410.
[4] M. Liu, M.E. Lynch, K. Blinn, F.M. Alamgir, Y. Choi, Materials Today, 14 (2011) 534-546.
[5] L. Yang, Y. Choi, W. Qin, H. Chen, K. Blinn, M. Liu, P. Liu, J. Bai, T.A. Tyson, M. Liu, Nat Commun, 2 (2011) 357.
[6] L. Yang, S. Wang, K. Blinn, M. Liu, Z. Liu, Z. Cheng, M. Liu, Science, 326 (2009) 126-129.
[7] D. Ding, X. Li, S.Y. Lai, K. Gerdes, M. Liu, Energy Environ Sci, 7 (2014) 552-575.
[8] H. Yokokawa, H.Y. Tu, B. Iwanschitz, A. Mai, J Power Sources, 182 (2008) 400-412.
[9] Fuel Cells Bulletin, 2004 (2004) 1.
[10] J.A. Schuler, Z. Wuillemin, A. Hessler-Wyser, C. Comminges, N.Y. Steiner, J. Van herle, Journal of Power Sources, 211 (2012) 177-183.
[11] J.A. Schuler, H. Yokokawa, C.F. Calderone, Q. Jeangros, Z. Wuillemin, A. Hessler-Wyser, J. Van Herle, J Power Sources, 201 (2012) 112-120.
[12] E. Konysheva, H. Penkalla, E. Wessel, J. Mertens, U. Seeling, L. Singheiser, K. Hilpert, J Electrochem Soc, 153 (2006) A765-A773.
[13] S.P. Jiang, J.P. Zhang, X.G. Zheng, J Eur Ceram Soc, 22 (2002) 361-373.
[14] S.P. Jiang, S. Zhang, Y.D. Zhen, J Mater Res, 20 (2005) 747-758.
[15] S.P. Jiang, Y.D. Zhen, S. Zhang, J Electrochem Soc, 153 (2006) A1511-A1517.
[16] Y.D. Zhen, A.I.Y. Tok, F.Y.C. Boey, S.P. Jiang, Electrochem Solid St, 11 (2008) B42-B46.
[17] S.P. Jiang, Y.D. Zhen, Solid State Ionics, 179 (2008) 1459-1464.
[18] T. Komatsu, H. Arai, R. Chiba, K. Nozawa, M. Arakawa, K. Sato, Electrochem Solid St, 9 (2006) A9-A12.
[19] M.K. Stodolny, B.A. Boukamp, D.H.A. Blank, F.P.F. van Berkel, J Electrochem Soc, 158 (2011) B112-B116.
[20] M.K. Stodolny, B.A. Boukamp, D.H.A. Blank, F.P.F. van Berkel, J Power Sources, 196 (2011) 9290-9298.
[21] M.K. Stodolny, B.A. Boukamp, D.H.A. Blank, F.P.F. van Berkel, J Power Sources, 209 (2012) 120-129.
[22] D. Ding, B. Liu, Z. Zhu, S. Zhou, C. Xia, Solid State Ionics, 179 (2008) 896-899.
[23] D. Ding, B.B. Liu, M.Y. Gong, X.B. Liu, C.R. Xia, Electrochim Acta, 55 (2010) 4529-4535.
[24] M.F. Liu, D. Ding, K. Blinn, X.X. Li, L.F. Nie, M.L. Liu, Int J Hydrogen Energ, (2012).
[25] J.D. Kim, G.D. Kim, J.W. Moon, Y.I. Park, W.H. Lee, K. Kobayashi, M. Nagai, C.E. Kim, Solid State Ionics, 143 (2001) 379-389.
[26] S.Z. Wang, Y. Jiang, Y.H. Zhang, J.W. Yan, W.Z. Li, Solid State Ionics, 113 (1998) 291-303.

[27] M.J. Jorgensen, M. Mogensen, J Electrochem Soc, 148 (2001) A433-A442.
[28] K.Q. Huang, P.Y. Hou, J.B. Goodenough, Solid State Ionics, 129 (2000) 237-250.
[29] J.W. Fergus, Mat Sci Eng A-struct, 397 (2005) 271-283.
[30] S. Fontana, R. Amendola, S. Chevalier, P. Piccardo, G. Caboche, M. Viviani, R. Molins, M. Sennour, J Power Sources, 171 (2007) 652-662.
[31] S.P.S. Badwal, R. Deller, K. Foger, Y. Ramprakash, J.P. Zhang, Solid State Ionics, 99 (1997) 297-310.
[32] J.J. Bentzen, J.V.T. Hogh, R. Barfod, A. Hagen, Fuel Cells, 9 (2009) 823-832.
[33] J.A. Schuler, Z. Wuillemin, A. Hessler-Wyser, C. Comminges, N.Y. Steiner, J. Van Herle, J Power Sources, 211 (2012) 177-183.
[34] Z. Zhao, L. Liu, X. Zhang, W. Wu, B. Tu, D. Ou, M. Cheng, J Power Sources, 222 (2013) 542-553.
[35] X. Li, K. Blinn, Y. Fang, M. Liu, M.A. Mahmoud, S. Cheng, L.A. Bottomley, M. El-Sayed, M. Liu, Phys Chem Chem Phys, 14 (2012) 5919-5923.
[36] L. Martin-Carron, A. de AndrÃ©s, M.J. MartÃnez-Lope, M.T. Casais, J.A. Alonso, Physical Review B, 66 (2002) 174303.
[37] H.W. Abernathy, E. Koep, C. Compson, Z. Cheng, M. Liu, Journal of Physical Chemistry C, 112 (2008) 13299-13303.
[38] B.P. Barbero, J.A. Gamboa, L.E. Cadus, Applied Catalysis B-Environmental, 65 (2006) 21-30.
[39] L.W. Tai, M.M. Nasrallah, H.U. Anderson, D.M. Sparlin, S.R. Sehlin, Solid State Ionics, 76 (1995) 273-283.
[40] H.W. Abernathy, E. Koep, C. Compson, Z. Cheng, M.L. Liu, J Phys Chem C, 112 (2008) 13299-13303.
[41] S.P. Jiang, Y. Zhen, Solid State Ionics, 179 (2008) 1459-1464.

Acronyms

SOFC: solid oxide fuel cell
YSZ: yttria-stabilized zirconia
SDC: samarium doped ceria with chemical formula $Sm_{0.2}Ce_{0.8}O_{1.95-\delta}$
LSM: the cathode material with chemical formula $La_xSr_{1-x}MnO_{3-\delta}$
LSCF: the cathode material with chemical formula $La_{0.6}Sr_{0.4}Co_{0.2}Fe_{0.8}O_{3-\delta}$
SSC: the cathode materials with chemical formula $Sm_{0.5}Sr_{0.5}CoO_{3-\delta}$
LCC: the cathode material with chemical formula $La_{0.4875}Ca_{0.0125}Ce_{0.5}O_{2-\delta}$
PSM: the cathode material with chemical formula $Pr_xSr_{1-x}MnO_{3-\delta}$
PNM: the cathode material with chemical formula $Pr_2Ni_{1-x}Mn_xO_{4-\delta}$
PSCM: the cathode material with chemical formula $PrSrCoMnO_{6-\delta}$
XRD: x-ray diffraction
SEM: Scanning electron microscopy
TEM: Transmission electron microscopy
SERS: surface enhanced Raman spectroscopy
XAS: x-ray absorption spectroscopy
XANES: x-ray absorption near-edge spectroscopy
EXAFS: extended x-ray absorption fine structure
FT: Fourier-transformed
OCV: open circuit voltage
ORR: oxygen reduction reaction
R_p: interfacial polarization resistance
MSRI: Materials System and Research, Incorporated